Okamoto and Oyanagi
Progress in Earth and Planetary Science (2023) 10:39
https://doi.org/10.1186/s40645-023-00568-w

Progress in Earth and Planetary Science

REVIEW

Open Access

Si- versus Mg-metasomatism at the crust–mantle interface: insights from experiments, natural observations and geochemical modeling

Atsushi Okamoto[1*] and Ryosuke Oyanagi[2,3]

Abstract

The slab–mantle interface in subduction zones is one of the geological boundaries with the most significant chemical potential gradients, which leads to fluid-mediated metasomatic reactions and chemical transport. As subducting sediment and basaltic crust often contain silica in various forms, the Si-metasomatism of mantle rocks is thought to occur along the subduction zone interface. However, growing evidence from the geochemistry of altered rocks and thermodynamic modelling has revealed the presence of multi-component fluids at the slab interface. Here, we review the laboratory experiments, geochemical models, and natural observations that improve our understanding of mass transport and metasomatic reactions at the crust–mantle interface, focusing on the relative mobility of Mg and Si. Hydrothermal experiments using analogues for the boundary between mantle (olivine) and crust (quartz or plagioclase) under vapor-saturated pressures indicate that Si is preferentially transported from crust to mantle, whereas Mg is immobile. This result is consistent with the distribution of talc rocks in oceanic lithosphere. On the other hand, at the contact between ultramafic (e.g., serpentinite) and crustal (pelitic schist or basaltic rocks) rocks in high-pressure metamorphic terranes, a large volume of chlorite rocks form in the crustal rocks, and the volume of chlorite often exceeds talc in serpentinites. Geochemical modeling reveals that in the shallow part of a subduction zone, the dissolved Si content of fluids in equilibrium with pelitic schist ($C_{Si,crust}$) is significantly higher than the dissolved Mg content of fluids in equilibrium with mantle peridotite ($C_{Mg,mantle}$); however, $C_{Mg,mantle}$ becomes dominant at depth, resulting in the Mg-metasomatism of crustal rocks to form chlorite rocks. This Mg-metasomatism is more widespread in warmer subduction zones (e.g., the Nankai and Cascadia subduction zones) than in colder subduction zones (e.g., in Northeast Japan). In addition, the infiltration of CO_2-bearing fluid can form talc (along with carbonates) in ultramafic rocks without Si-metasomatism. Variations in the relative mobility of Si and Mg at the subduction zone interface produce variations in the overall solid volume change of mantle (expansion or contraction), the types of sheet silicates (talc versus chlorite), and the fluid budget (dehydration or hydration) during metasomatic reactions, which affects the pore fluid pressure, frictional strength of the subduction megathrust, and the location of seismicity around the mantle wedge corner.

Keywords Element mobility, Metasomatism, Crust–mantle interface, Fluid, Chloritization

*Correspondence:
Atsushi Okamoto
atsushi.okamoto.d4@tohoku.ac.jp
Full list of author information is available at the end of the article

1 Introduction

The increasing amount of thermodynamic data on rock-forming minerals has made it possible to predict stable mineral assemblages in the Earth's interior based on the bulk rock chemistry and thermal structure. The thermodynamic stability of hydrous minerals along the subduction interface can be compared with geophysical observations, including the seismic velocity structure and hypocenter distributions, and this has increased our understanding of the importance of volatile species in controlling seismicity, magmatism, and global chemical recycling (e.g., Hacker et al. 2003; Kita et al. 2006; van Keken et al. 2011; Scambelluri et al. 2019). In contrast to the well-established thermodynamic models of metamorphic and mantle rocks with fixed bulk chemistry, our understanding of the chemistry of subduction zone fluids is limited, including our knowledge of the speciation of aqueous species, the redox conditions, and the metasomatic reactions that occur during the transport of elements. Recent detailed analyses of natural high-pressure metamorphic rocks and progress in acquiring thermodynamic data for aqueous species suggest that multi-component fluids have a strong influence on the mechanical and chemical properties of the slab–mantle interface (e.g., Bebout and Penninston-Dorland 2016; Galvez et al. 2016; Scambelluri et al. 2019; Tarling et al. 2019b; Hoover et al. 2022).

One of the most distinct chemical boundaries in the Earth's interior is the interface between a subducting slab and the overlying mantle wedge. The dehydration of subducting sediments and basaltic crust produces aqueous fluids that result in extensive mantle hydration (i.e., serpentinization) at the slab–mantle interface and in the forearc mantle wedge (Hyndman and Peacock 2003). This hydration is observed as low-seismic velocity zones and seismic anisotropy in subduction zones (e.g., Bostock et al. 2002; Katayama et al. 2009).

In addition to hydration and dehydration, the aqueous species dissolved in the fluids can generate significant chemical and mechanical changes at the plate interface. Silica, in particular, is thought to be a key species, as the crustal rocks such as subducting sediments and metabasaltic rocks commonly contain silica minerals, whose solubility in water increases with temperature and pressure (Manning 1994). We use the term "crustal rocks" to refer to oceanic sedimentary and mafic crustal rocks throughout the manuscript. The precipitation of quartz may control the pore fluid pressure along the subduction zone interface and may influence the recurrence interval of subduction zone seismicity (e.g., Audet and Bürgmann 2014; Saishu et al. 2017). In contrast to crustal rocks, mantle peridotite has Si activities that are several orders of magnitude lower than quartz solubility (Frost and Beard 2007); therefore, it is thought that Si-metasomatism of mantle rocks (peridotite or serpentinite) to form talc occurs pervasively at the slab–mantle interface (Manning 1995, 1997; Peacock 1999; Hyndman and Peacock 2003). Talc is the mechanically weakest mineral in mantle, and Si-metasomatism potentially has a large influence on the seismic properties of the slab–mantle interface and its mechanical coupling (Moore and Rymer 2007; Hirauchi et al. 2012; 2016, 2020; Tarling et al. 2019b). However, it is difficult to constrain the thickness and distribution of metasomatic layers solely from geophysical observations (Nagaya et al. 2020).

High-pressure metamorphic terranes often contain both ultramafic mantle rocks and sedimentary and mafic rocks. Blocks of crustal rocks occur in a serpentinite matrix in mélange zones near the slab–mantle interface, and ultramafic rocks occur as blocks and lenses within the metamorphosed crustal rocks (e.g., Bebout and Penniston-Dorland 2016). At the contact between mantle and crustal rocks in these terranes, metasomatic reaction zones are commonly developed, which comprise talc rock, chlorite rock, tremolite/actinolite rock, albitized rock, and carbonate rock (e.g., Miller et al. 2009; Mori et al. 2014; Tarling et al. 2019b; Okamoto et al. 2021; Codillo et al. 2022a; Oyanagi et al. 2023). The occurrence of such reaction zones indicates the transport of elements (e.g., Mg, Ca, Al, and CO_2 in addition to Si) in both directions between crust and mantle. In particular, Mg is the dominant component of mantle rocks, and recent studies have highlighted the mobility of Mg from mantle to crust and the formation of chlorite rock (e.g., Okamoto et al. 2021; Codillo et al. 2022a; Oyanagi et al. 2023).

The development of reaction zones between olivine (Ol) and quartz (Qz) has been investigated as an analogue of the metasomatic processes that occur between the upper mantle and pelitic sediments using diffusive transport models (Frantz and Mao 1979; Lichtner et al. 1986; Oyanagi et al. 2020). A small number of experimental studies have been conducted on the development of metasomatic zones using analogues of the crust–mantle interface (Oyanagi et al. 2015, 2018, 2020). These studies have suggested that the relative mobility of Si and Mg via diffusion in aqueous fluids plays an important role in the development of metasomatic reaction zones at the crust–mantle interface. In particular, the hydrothermal experiments on an analogue crust–mantle boundary suggest the preferential mobility of Si to form talc in mantle rocks (Oyanagi et al. 2015, 2020). However, as such experiments have been conducted only under vapor-saturated conditions, the applicability of the estimated Si and Mg mobilities at elevated temperatures and pressures is unclear.

Recently, the applicability of thermodynamic data for aqueous species (ions and complexes) has been extended to mantle pressures based on a new model of the dielectric constant of water (the Deep Earth Water (DEW) Model; Sverjensky et al. 2014; Huang and Sverjensky 2019). The DEW model extends the Helgeson–Karkham–Flowers equation of state for the free energy of aqueous species to 6 GPa and 1200 °C (Sverjensky et al. 2014). This database has enabled studies of fluid–rock interaction in subduction zones, including the evolution of multi-component fluid chemistry from shallow to deep in subduction zones (Galvez et al. 2015, 2016; Connolly and Galvez 2018) and geochemical modeling of the development of metasomatic reaction zones at the slab–mantle interface (Okamoto et al. 2021; Codillo et al. 2022a, b) and the behavior of CHO fluids related to deep fault zones (Vitale-Brovarone et al. 2020). Based on thermodynamic model of fluid-rock interaction (reaction path modeling) using the DEW model, Codillo et al. (2022b) suggested that chlorite rocks in the mantle commonly form in warm subduction zones, whereas the formation of talc in the mantle occurs preferentially in cold subduction zones.

Here we review multiple approaches for improving our understanding of metasomatic reactions and chemical transport at the crust–mantle interface, including hydrothermal experiments, natural observations, and geochemical modeling. We focus on the relative mobilities of Mg (the dominant element in mantle) and Si (the dominant element in crust) at the crust–mantle interface. First, we present the models and experimental data on the fundamental metasomatic reactions between olivine and quartz or plagioclase and introduce the effects of CO_2-bearing fluids on the alteration of ultramafic rocks. Second, we review representative occurrences of metasomatic reaction zones at the contact between crustal and mantle rocks in metamorphic terranes. Third, we present the results of geochemical modeling studies on the metasomatic zones using recently updated thermodynamic data. We include new geochemical calculations to show the variations in the relative mobility of Mg and Si along the various subduction zone interfaces, and discuss the potential impact of Mg- versus Si-metasomatism on the mechanical and hydrological properties of the subducting plate interface.

2 Metasomatic reactions and hydrothermal experiments

2.1 Metasomatic reactions between crustal and ultramafic rocks

Metasomatism is a reaction induced by chemical transfer involving fluids. Metasomatic reaction zones often occur at lithological contacts, where diffusion is enhanced, and in places where infiltration of the external fluids occurs (e.g., Bebout and Penniston-Dorland 2016). Metasomatic reactions are enhanced by mechanical mixing, where different rocks are tectonically juxtaposed (e.g., in a mélange zone). Metasomatism is often observed in mantle rocks where they are in contact with crustal rocks. The dominant metasomatic agents in aqueous fluids include Si, Ca, and CO_2, and typical metasomatic reactions in the hydrated mantle (serpentinite) include the following.

Si-metasomatism of serpentinite:

$$\underset{\text{Serpentine}}{Mg_3Si_2O_5(OH)_4} + 2SiO_2(aq) \rightarrow \underset{\text{Talc}}{Mg_3Si_4O_{10}(OH)_2} + H_2O \quad \text{(R1)}$$

Ca–Si-metasomatism of serpentinite:

$$5\underset{\text{Serpentine}}{Mg_3Si_2O_5(OH)_4} + 14SiO_2(aq) + 6CaO(aq) \rightarrow 3\underset{\text{Tremolite}}{Ca_2Mg_5Si_8O_{22}(OH)_2} + 7H_2O \quad \text{(R2)}$$

CO_2-metasomatism of serpentinite:

$$2\underset{\text{Serpentine}}{Mg_3Si_2O_5(OH)_4} + 3CO_2(aq) \rightarrow 3\underset{\text{Magnesite}}{MgCO_3} + \underset{\text{Talc}}{Mg_3Si_4O_{10}(OH)_2} + 3H_2O \quad \text{(R3)}$$

Antigorite, the high-temperature polymorph of serpentine, has a slightly different chemical formula [$Mg_{48}Si_{34}O_{85}(OH)_{62}$] to that of low-temperature serpentine minerals [lizardite, chrysotile; $Mg_3Si_2O_5(OH)_4$]. However, as the metasomatic reactions are almost identical, we describe them using a chemical formula of $Mg_3Si_2O_5(OH)_4$.

Mg-metasomatism of crustal rocks to form chlorite rock has been reported at some natural examples of the crust–mantle boundary (e.g., Scambelluri et al. 1999). For example, the chloritization of plagioclase (albite) in an Al-fixed reference frame can be written as follows:

$$\underset{\text{Albite}}{2NaAlSi_3O_8} + 5MgO(aq) + 4\,H_2O \rightarrow \underset{\text{Chlorite}}{Mg_5Al_2Si_3O_{10}(OH)_8} + 3SiO_2(aq) + Na_2O(aq) \quad \text{(R4)}$$

However, Mg-metasomatism has attracted less attention than Si-metasomatism, and it is still not clear how common Mg-metasomatism is in various geological settings.

In this section, we review numerical models and experimental studies of the development of metasomatic reaction zones in simple systems as analogues of the crust–mantle boundary. We show that Si-metasomatism dominates over Mg-metasomatism in experiments under hydrothermal conditions (mostly vapor saturated), in contrast to natural examples from metamorphic terranes described in later sections. Then, we describe experiments showing the effects of CO_2-rich fluids on the development of metasomatic zones in ultramafic rocks.

2.2 A typical model for the development of metasomatic reaction zones

Figure 1a shows the stabilities of mantle-forming minerals in the $MgO–SiO_2–H_2O$ system with varying SiO_2 activity ($a_{SiO2,aq}$) and temperature. The stable hydrous minerals do not change significantly between 0.1 and 1.0 GPa. With increasing silica activity, the stable hydrous mineral changes from brucite (Brc) to serpentine (Srp) to talc (Tlc). The hydration reactions of olivine and orthopyroxene (Opx) can be written as follows:

$$\underset{\text{Olivine}}{2Mg_2SiO_4} + 3H_2O \rightarrow \underset{\text{Serpentine}}{Mg_3Si_2O_5(OH)_4} + \underset{\text{Brucite}}{Mg(OH)_2} \quad \text{(R5)}$$

$$\underset{\text{Orthopyroxene}}{6MgSiO_3} + 3H_2O \rightarrow \underset{\text{Serpentine}}{Mg_3Si_2O_5(OH)_4} + \underset{\text{Talc}}{Mg_3Si_4O_{10}(OH)_2} \quad \text{(R6)}$$

Srp + Brc equilibrium yields 2–3 orders of magnitude lower silica activity than Srp + Tlc equilibrium (Fig. 1a). Olivine appears at higher temperatures with increasing silica activity from the Srp + Brc + Ol invariant point to the Srp + Tlc + Ol invariant point (Fig. 1a). The silica activity for Qz-saturated aqueous fluid is always higher than the silica activity at Tlc–Srp equilibrium (Fig. 1a); this Si activity gradient is a typical driving force for the Si-metasomatism of mantle rocks at the crust–mantle interface (Frost and Beard 2007; Manning 1995; Oyanagi et al. 2015; 2020).

The development of a metasomatic reaction zone between olivine and quartz has been modeled as an example of metasomatism in a binary system resulting from intergranular diffusion (Fig. 1b; Frantz and Mao 1979; Lichtner et al. 1986). The model assumes local equilibrium, where individual minerals are immediately precipitated when they become supersaturated in the fluid, and thus the diffusion of Si and Mg in aqueous fluids is the rate-limiting process. By solving for a moving boundary numerically, Lichtner et al. (1986) showed that monomineralic reaction zones developed in order of their silica activity: a talc zone is developed near the Ol–Qz contact in the Ol-hosted region, and a serpentine zone is developed far from the Ol–Qz contact in the Ol-hosted region (Fig. 1b). A small amount of talc also forms in the Qz-hosted region. As the Si concentration in equilibrium

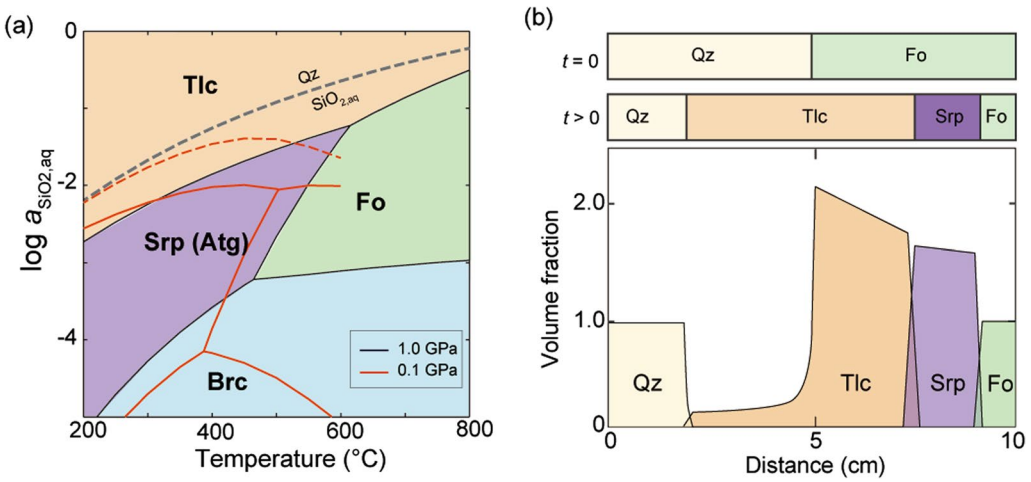

Fig. 1 **a** Mineral stability with temperature and silica activity for the $MgO–SiO_2–H_2O$ system at 0.1 and 1.0 GPa. The dashed lines indicate the solubility of quartz in water. Fo: forsterite, Srp: serpentine, Atg: antigorite, Brc: brucite, Tlc: talc, Qz: quartz. **b** Results of a typical diffusion–reaction model by Lichtner et al. (1986) for the development of reaction zones between forsterite and quartz in the $MgO–SiO_2–H_2O$ system. Distinct talc and serpentine zones developed in the Ol-hosted region, whereas a small talc zone formed in the Qz-hosted region. The volume fraction is defined as the ratio of the volume of the mineral to the initial solid volume

with quartz is assumed to be higher than the Mg concentration in equilibrium with olivine, the diffusive flux of Si is higher than that of Mg. This asymmetric diffusive flux results in a large solid volume increase in the serpentine and talc zones in the Ol-hosted region, whereas a significant solid volume loss in the talc zone in the Qz-hosted region (Fig. 1b). These pioneering modeling studies show that a difference in the diffusive fluxes of Si and Mg produces asymmetric widths and porosities in the metasomatic reaction zones on either side of the Ol–Qz contact; however, the Si and Mg concentrations in these models were approximated without any experimental data.

2.3 Hydrothermal experiments on bimetasomatism by intergranular diffusion

Experiments producing metasomatic reaction zones between two lithologies or minerals are limited. However, several hydrothermal experiments have been conducted using mineral powders to study the contact between olivine and more SiO_2-rich minerals, including Ol–Opx (Ogasawara et al. 2013), Ol–Qz (Oyanagi et al. 2015, 2020), and Ol–plagioclase (Pl, Oyanagi et al. 2018) pairs. These experiments were conducted at 230–300 °C and under vapor-saturated pressures (P_{sat}, ~ 3–10 MPa).

2.3.1 Olivine–orthopyroxene system

Ogasawara et al. (2013) conducted hydrothermal experiments in the Ol–Opx–H_2O system at 250 °C and P_{sat} (4 MPa). Ol powder was sandwiched by Opx powder and placed in the inner tube. In the Ol–Opx system, serpentine was formed both in the Ol- and Opx-hosted regions, and brucite and talc were not identified (Fig. 2a). The amount of serpentine formed was spatially uniform in the Opx-hosted region, whereas in the Ol-hosted region, the serpentinization was most intense at the contact with the orthopyroxene and decreased gradually with increasing distance from the contact. This pattern is explained by the following coupled silica-releasing and silica-consuming reactions in the Mg-fixed reference flame:

Silica-consuming olivine reaction

$$\underset{\text{Olivine}}{3Mg_2SiO_4} + 4H_2O + SiO_2(aq) \rightarrow \underset{\text{Serpentine}}{2\,Mg_3Si_2O_5(OH)_4} \quad \text{(R7)}$$

Silica-releasing orthopyroxene reaction

$$\underset{\text{Orthopyroxene}}{3MgSiO_3} + 2H_2O \rightarrow \underset{\text{Serpentine}}{Mg_3Si_2O_5(OH)_4} + SiO_2(aq) \quad \text{(R8)}$$

A 1-dimensional reaction–diffusion model (Fig. 2a) shows that the olivine serpentinization reaction rate (R7) is ~ 14 times higher than the orthopyroxene serpentinization reaction rate (R8) (Ogasawara et al. 2013). Coupled serpentinization reactions between olivine and orthopyroxene are commonly observed during the serpentinization of harzburgite in the oceanic lithosphere (Schwarzenbach et al. 2016) and forearc ophiolites (Dandar et al. 2019), suggesting the importance of Si transport during serpentinization.

2.3.2 Olivine–quartz system

Oyanagi et al. (2020) conducted hydrothermal experiments using layers of quartz and olivine powder at 300 °C and P_{sat} (8.58 MPa). Reaction zones only developed in the Ol-hosted region and changed from Tlc + Srp to Srp to Srp + Brc + Mag with increasing distance from the Ol–Qz contact (Fig. 2b). At the contact, talc formed around olivine grains, whereas quartz grains were dissolved without producing any reaction products. The formation of brucite in the Ol-hosted region means there was a silica activity gradient of three orders of magnitude over a distance of only 10 mm (Fig. 1a). Oyanagi et al. (2020) modeled the reaction systems involving olivine, brucite, serpentine, and talc assuming that they were controlled only by Si from the Qz-hosted region. In addition to reactions R1 and R7, the overall reactions in the Mg-fixed reference frame were as follows:

(See figure on next page.)

Fig. 2 Hydrothermal experiments on metasomatic reactions. **a** Ol–Opx contact at 250 °C and P_{sat} (modified after Ogasawara et al. 2013). Left panel: photograph of the reaction zones at the Ol–Opx contacts after 1520 h. Right panel: ratio of the volume of serpentine to the total solid volume (V_{srp}/V_{solid}) versus distance from the tube top, along with the V_{srp}/V_{solid} ratio predicted by the reaction–diffusion model (red curves). **b** Ol–Qz contact at 300 °C and P_{sat} (modified after Oyanagi et al. 2020). Top: photograph of the reaction zones at the Ol–Qz contact after 3258 h. Bottom: Back-scattered electron (BSE) images of the products at 0 and 10 mm from the Ol–Qz contact. **c** Ol–Pl contact at 250 °C and P_{sat} (modified after Oyanagi et al. 2018). Top: photograph of the reaction zones at the Ol–Pl contact after 7980 h with the positions of Al and Ca, Si, and hydration fronts. The Si front is identified by the appearance of brucite and magnetite, and the Ca and Al front is identified by the chemical compositions of serpentine minerals. Bottom: BSE images of the products at the Ol–Pl contact (left) and of serpentine with Al zoning (right). **d** Temperature–X_{CO2} diagram at 200 MPa showing the equilibrium phase relationship in the MgO–SiO_2–H_2O–CO_2 system for an MgO:SiO_2 ratio of 2:1 (modified after Johannes 1969). **e** BSE image and interpretation of a harzburgite–CO_2–H_2O experiment at 600 °C and 2.0 GPa after 192 h (modified after Sieber et al. 2022). **f** X-ray computed tomographic image of the product of a serpentinite–CO_2–H_2O experiment at 700 °C and 2.5 GPa after 96 h (modified after Sieber et al. 2020). Ol: olivine, Opx: orthopyroxene, Qz: quartz, Srp: serpentine, Brc: brucite, Pl: plagioclase, Mag: magnetite, Ca-Sap: Ca-saponite, Mgs: magnesite, Tlc: talc, Atg: antigorite, Cb: carbonate, Vac: vacancy

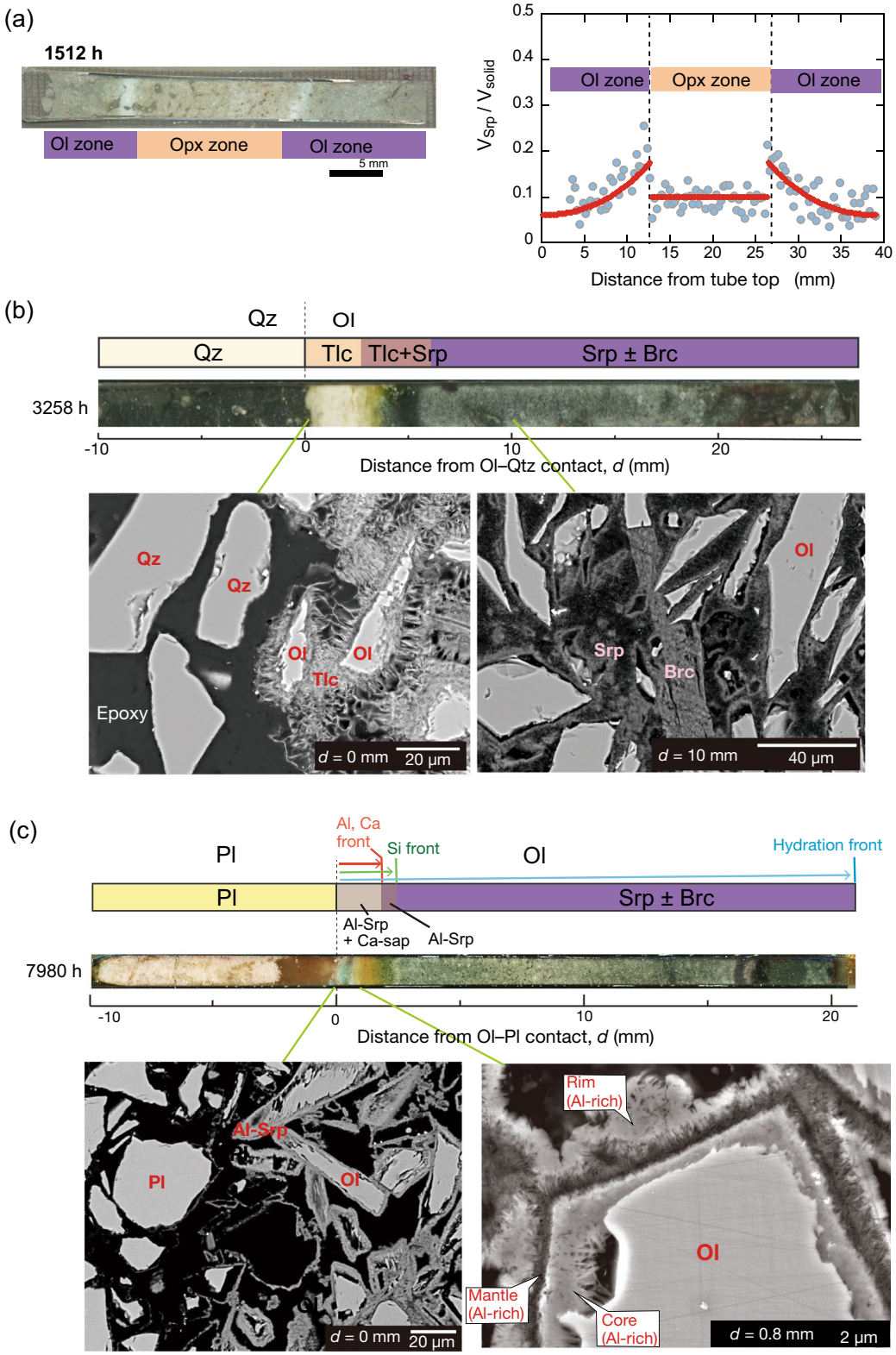

Fig. 2 (See legend on previous page.)

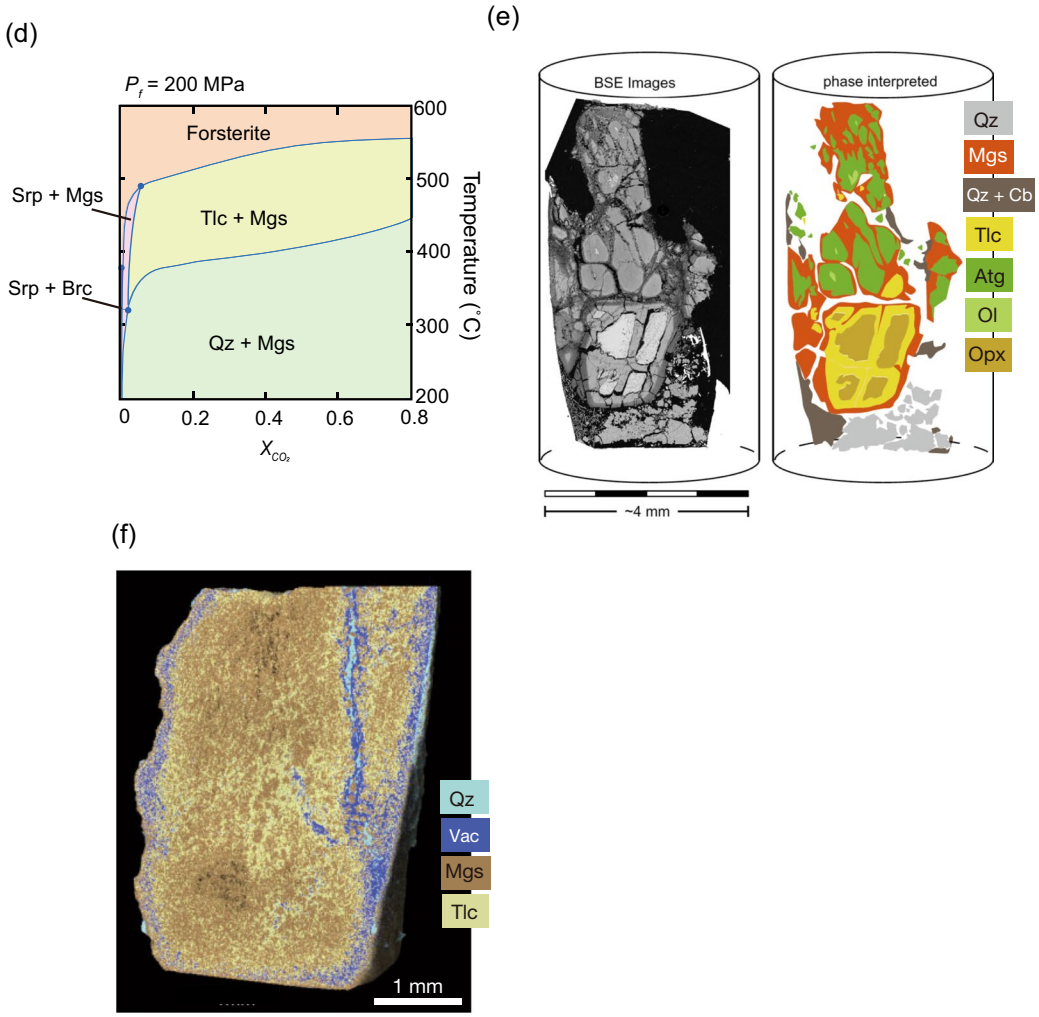

Fig. 2 continued

$$3Mg_2SiO_4 + 5SiO_2(aq) + 2H_2O \rightarrow 2Mg_3Si_4O_{10}(OH)_2 \quad \text{(R9)}$$
Olivine → Talc

$$Mg_2SiO_4 + 2H_2O \rightarrow 2Mg(OH)_2 + SiO_2(aq) \quad \text{(R10)}$$
Olivine → Brucite

$$Mg_3Si_4O_{10}(OH)_2 + H_2O \rightarrow Mg_3Si_2O_5(OH)_4 + 2SiO_2(aq) \quad \text{(R11)}$$
Talc → Serpentine

$$3Mg(OH)_2 + 2SiO_2(aq) \rightarrow Mg_3Si_2O_5(OH)_4 + H_2O \quad \text{(R12)}$$
Brucite → Serpentine

$$Mg_3Si_2O_5(OH)_4 + H_2O \rightarrow 3Mg(OH)_2 + 2SiO_2(aq) \quad \text{(R13)}$$
Serpentine → Brucite

The reactions R7 (Ol–Srp), R9 (Ol–Tlc), and R10 (Ol–Brc) are olivine hydration, whereas the reactions R1 (Srp–Tlc) and R12 (Brc–Srp) are characterized by the dehydration of pre-existing hydrous minerals. This means that either hydration or dehydration can occur during the Si-metasomatism of mantle rocks (Oyanagi et al. 2015; 2020; Okamoto et al. 2021). The silicification of brucite (R12) is known as an important step in the serpentinization of olivine (Bach et al. 2006; Tutolo et al. 2018).

The preferential development of a reaction zone in the Ol-hosted region was also found in the Ol–Qz experiments under highly alkaline conditions using a NaOH aqueous fluid (pH = 13.8 at 25 °C) at 250 °C and P_{sat} (3.98 MPa, Oyanagi et al. 2015). Due to the dissolved NaOH, instead of talc, Na-smectite was formed in the Si-metasomatic zone that developed in the olivine-hosted region. The Si-metasomatic front migrates ~ 10 times faster under highly alkaline conditions (Oyanagi et al. 2015) than under near-neutral pH conditions (Oyanagi et al. 2020). The dominant aqueous silica species is $SiO_{2,aq}$ in the case of near-neutral pH or acidic conditions,

whereas $HSiO_3^-$ is dominant under highly alkaline conditions (pH > ~10; e.g., Shibuya et al. 2010). Therefore, the faster migration of the Si-metasomatic front under alkaline conditions (Oyanagi et al. 2015) than at near-neutral pH (Oyanagi et al. 2020) is probably due to the larger diffusive flux due to the higher Si concentration gradient in the former case.

2.3.3 Olivine–plagioclase system

Gabbroic rocks in the lower crust are composed mainly of plagioclase and clinopyroxene (Cpx), and lack quartz. The aqueous fluids buffered by these rocks have higher dissolved Ca and Al contents as well as Si contents. The mobility of Al was recognized in the serpentinization of olivine adjacent to clinopyroxene or plagioclase in harzburgite, olivine gabbro, and troctolites (Beard et al. 2009; Schwarzenbach et al. 2016; Oyanagi et al. 2018; Yoshida et al. 2020).

Oyanagi et al. (2018) conducted hydrothermal experiments on the Ol–Pl–H_2O system at 230 °C and P_{sat} (2.8 MPa), and identified the Al–Si-metasomatic zones in the experimental products (Fig. 2c). Instead of talc observed in the Ol-Qz experiments, Al-rich serpentine formed in the Ol-hosted region close to the Ol–Pl contact, and no reaction products were observed in the Pl-hosted region. The Si-metasomatic front migrated farther than the Al metasomatic front. The distinct Al zoning developed in the Al-rich serpentine aggregate that replaced the olivine crystal, with Al-rich cores, Al-poor mantles, and Al-rich rims (Fig. 2c), similar to the Al-zoning observed in areas of serpentine mesh texture in troctolite (Oyanagi et al. 2018; Yoshida et al. 2020). This Al zoning is produced in response to the migration of an Al-metasomatic front, with the Al-poor serpentine forming during the early stages, followed by coupled olivine replacement and overgrowth by Al-rich serpentine. In some experiments on olivine hydration with Al-oxides, chlorite was formed instead of Al-rich serpentine (Andreani et al. 2013). Ol–Pl–H_2O experiments suggest differences in the mobility of Si, Al, Ca, and Mg (Fig. 2c).

2.4 Experimental studies of metasomatic reactions in ultramafic rock–H_2O–CO_2 systems

Equilibrium phase relationships in the MgO–SiO_2–H_2O–CO_2 system have been investigated experimentally (e.g., Johannes 1969). Figure 2d shows a temperature–X_{CO2} [$=CO_2/(H_2O+CO_2)$] diagram at 200 MPa for a bulk composition of forsterite (MgO:SiO_2 = 2:1; Johannes 1969). Serpentine and brucite only appear at low X_{CO2} values (< 0.1). At higher X_{CO2} values ($0.1 < X_{CO2} < 0.9$), the assemblage changes from Qz + magnesite (Mgs) to Tlc + Mgs with increasing temperature. At temperatures of ~ 300–450 °C, the mineral assemblage changes from Srp + Brc, through Srp + Mgs and Tlc + Mgs, to Qz + Mgs with increasing X_{CO2} at constant P–T conditions (Fig. 2d). This trend represents the mineralogical sequence produced by infiltration of CO_2-rich fluids, although the exact T–X_{CO2} stability fields of individual assemblages vary depending on pressure.

Numerous experiments on the carbonation of ultramafic rocks have been conducted to develop techniques for carbon dioxide capture and storage (CCS) in minerals and geological formations (e.g., Andreani et al. 2009; Klein et al. 2013; Lacinska et al. 2017). Most of these experiments were conducted at low temperatures and pressures (≲ 300 °C, < 50 MPa) and show that the carbonation of serpentine is several orders of magnitude slower than that of olivine or brucite (e.g., Kelemen et al. 2019). CCS studies are summarized in the review of Kelemen et al. (2019), and we briefly describe recent experimental studies on the metasomatic alteration of harzburgite and serpentinite blocks by the infiltration of CO_2–H_2O fluids at mantle wedge P–T conditions (Sieber et al. 2020; 2022). Metasomatic zonation has been produced in harzburgite, with antigorite forming around olivine and talc forming around orthopyroxene; both textures were surrounded by magnesite. Regions of Qz + Mgs and Qz were formed at the edges of the samples (Fig. 2e; Sieber et al. 2022). The hydration of harzburgite produced polygonal fractures, caused by hierarchical fracturing induced by solid volume-increasing reactions. In serpentinite composed mainly of antigorite, a uniform mixture of fine Tlc + Mgs crystals formed in the interior of serpentinite, with quartz forming preferentially at the edges of the serpentinite (Fig. 2f; Sieber et al. 2020). The extent of serpentinite carbonation (Sieber et al. 2020) was similar to that of olivine carbonation (Sieber et al. 2022) in experiments at mantle wedge conditions, in contrast to serpentine and olivine carbonation under low P–T conditions (Kelemen et al. 2019). Porosity networks developed in the products of serpentinite carbonation, particularly near quartz, suggesting a decrease in solid volume and chemical transport associated with the dehydration of serpentine (R3). Experiments using ultramafic samples (Sieber et al. 2020; 2022) show that characteristic mineral sequences are produced as a function of X_{CO2} and that significant Si and Mg transport are not always required during CO_2-metasomatism.

3 Natural metasomatic reaction zones upon the crust–mantle interface

The contacts between crustal rocks and mantle rocks are often exposed within the high-pressure metamorphic terranes and ophiolites. In some cases, serpentinite blocks

Table 1 Natural occurrences of metasomatic reaction zones at the contact between crust and mantle rocks

	Setting	Occurences	Metasomatic zones hosted by ultramafic rocks	Metasomatic zones hosted by crustal rocks	Serpentine minerals	Gain/loss during alteration of the ultramafic rock	Gain/loss during alteration of the ultramafic rock	References
Nishisonogi metamorphic rocks	Subduction zone	Serpentinite pods in pelitic schist	Mgs + Qz veins/ Tlc + Car (Act)/ Car + Qz	Chl/Ms/Ab	Atg	Gain: CO_2 Loss: Mg, Ca, H2O	Gain: Mg, Fe, H_2O Loss: Si, K, C	Mori et al. (2007)
Sanbagawa Belt (Higuchi body)	Subduction zone	Serpentinite block in pelitic schist	Car + Tlc veins/Act-Chl schist	Chl	Atg	Gain: Si, Ca, CO_2 Loss:Mg, H2O (n.a.)	Gain: Mg, H_2O Loss: Si, Na, K	Okamoto et al. (2021)
Sanbagawa Belt (Tomisato body)	Subduction zone	Serpentinite block in pelitic schist	Tlc + Chl/Tlc veins	Chl/Ms/Ab	Atg	Gain: Si, Ca, Al Loss:Mg, H2O	Gain: Mg, H_2O Loss: Si, Na, K	Oyanagi et al. (2023)
Livingstone fault	Tectonic fault between the Dun Mountain Ophiolite Belt and the Caples terrane	Schist blocks in Serpentine shear zone	Tr vein, Tlc veins/Tr	Rodingite pods (occationary)	Chry/Liz (minor Atg)	Gain: Si, Ca? (n.a.)	n.d	Tarling et al. (2019a, b)
Voltri massif	Oceanic lithosphere → Subduction zone	Metagabbro block in schistose serpentinite	No reaction zone (Tlc veins)	Ca-Amp + Chl/ Chl + Ca-Amp/Ep	Atg	n.a	Gain: Mg, H_2O Loss: Ca (Chl rock)	Collido et al. (2022b)
Flanciscan Complex (Jade Cove)	Oceanic lithosphere → Subduction zone	Serpentine melange	Tr + Chl, Chl + Tlc	Tr overgrowth + Chl	Liz/Chry → Atg	Gains: Si, Ca Loss: n.a	Gain: Mg? (n.a.)	King et al. (2003); Hirauchi etal. (2020)

Chl, chlorite; *Ms*, muscovite; *Ab*, albite; *Amp*, amphibole; *Ep*, epidote; *Atg*, antigorite; *Chry*, chrysotile; *Liz*, lizardite; *n.d.*, not described; *n.a.*, not analyzed qunatitatively

occur in schists, and in the other cases, the oceanic crustal rocks occur as blocks in the serpentinite mélange. Regardless their occurrences or origins (mantle wedge or oceanic lithosphere), the metasomatic reaction zones are commonly developed at the contact. In this section, we review natural examples of contacts between crustal and ultramafic rocks, focusing on Mg- and Si-metasomatism. Table 1 summarizes representative examples of reaction zones at crust–mantle interfaces. Figure 3 shows the *P*–*T* conditions of metasomatism in various locations along with the geotherm along the top of the slab in representative subduction zones (van Keken et al. 2018). Although there are large uncertainties in the *P*–*T* conditions of metasomatism, most are similar to those of the Nankai and Cascadia subduction zones (Fig. 3).

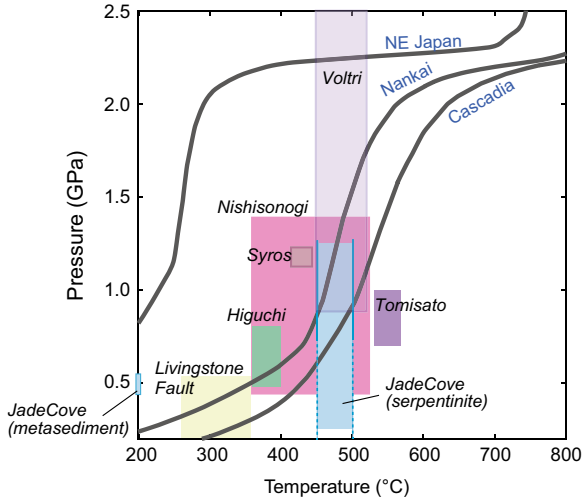

Fig. 3 *P*–*T* conditions of metasomatism in crustal and ultramafic rocks in various geological settings with the geotherm along the slab top in the NE Japan, Nankai, and Cascadia subduction zones calculated by van Keken et al. (2018). Data for the Higuchi (Okamoto et al. 2021) and Tomisato (Oyanagi et al. 2023) bodies in the Sanbagawa metamorphic belt in Japan, the Livingstone Fault in New Zealand (Tarling et al. 2019b), the Jade Cove mélange in the Franciscan Complex, USA (King et al. 2003), the Voltri Massif in the Ligurian Alps, Italy (Codillo et al. 2022a), the Nishisonogi metamorphic rocks (Mori et al. 2007), and Syros, Greece (Miller et al. 2009) are shown for comparison

3.1 Serpentinites in the Sanbagawa metamorphic belt

The Sanbagawa belt is a high-pressure metamorphic belt that extends for > 800 km along the Japanese Islands. The belt contains numerous ultramafic bodies and lenses (peridotite, serpentinite, tremolite (Tr)/actinolite (Act) rocks) of centimeters to kilometers in length (Aoya et al. 2013). In central Shikoku, these ultramafic bodies occur only at grades higher than the garnet zone (Aoya et al. 2013). This distribution of ultramafic bodies, combined with the depleted compositions of Cr-rich spinel and the bulk rock chemistry (Hattori et al. 2010; Kawahara et al. 2016; Okamoto et al. 2023), suggests that the ultramafic bodies were derived from the mantle wedge. The ultramafic bodies are extensively serpentinized with antigorite, and the hydration reactions were affected by external fluids at the margins of the bodies. For example, the km-scale serpentinite body in Central Shikoku (Shiraga body) only has an Atg–Brc assemblage in the interior of the body, whereas the marginal part of the body in contact with the pelitic schists lacks brucite and contains talc veins (Kawahara et al. 2016; Nagaya et al. 2022). The spatial variation in hydrous minerals probably reflects higher Si activity at the edge of the body, and that Si-metasomatism proceeded by infiltration of external fluids from the pelitic schists. Talc formation did not occur through the alteration of olivine (R8), but through the alteration of pre-existing serpentine (R12). This is consistent with the experiments in the Ol–Qz system (Oyanagi et al. 2015; 2020), where the hydration front (Srp + Brc) proceeded farther than the Si-metasomatic front (Tlc, Tlc + Srp; Fig. 2b). In this outcrop, the progress of Mg-metasomatism in the pelitic schist is unclear due to weathering.

3.1.1 Higuchi serpentinite body

The Higuchi body in the Kanto Mountains is a small (8 × 15 m) carbonated serpentinite body hosted by pelitic schist (Okamoto et al. 2021; Fig. 4a). The body is composed mainly of massive antigorite with no relic olivine, pyroxene, or brucite. The massive antigorite is cut by several types of Tlc–carbonates (Cb) (magnesite, dolomite (Dol), calcite (Cal)) veins that form branching fracture networks (Fig. 4b). In the interior of the body, the massive antigorite is cut by thin networks of Tlc–Mgs veins. The most distinct veins are filled with dolomite with a talc selvage (Fig. 4c). The Tlc–Cb veins record the progress of CO_2-metasomatism, similar to R3, with intense fracturing as observed in the experiments of Sieber et al. (2020) (Fig. 2f). The thickest veins are Dol–Cal veins with euhedral dolomite crystals and interstitial calcite, providing the temperature estimates by the Cal-Dol thermometry of 380–400 °C (Okamoto et al. 2021). The boundary of the serpentinite body is marked by reaction zones of ~ 50 cm thickness (Fig. 4a), with Act–chlorite (Chl) schist on the serpentinite side and chlorite rock on the pelitic shist side. The Act–Chl schist contains altered Cr-rich spinel, suggesting that it formed from serpentinite (Fig. 4d), whereas the partly chloritized rocks preserve the distinct textures of the pelitic schists, including graphite-rich layers and quartz veins with equigranular grains (Fig. 4e). Mass balance analysis of the alteration of pelitic schist to Chl rock indicates a loss of SiO_2, Na_2O,

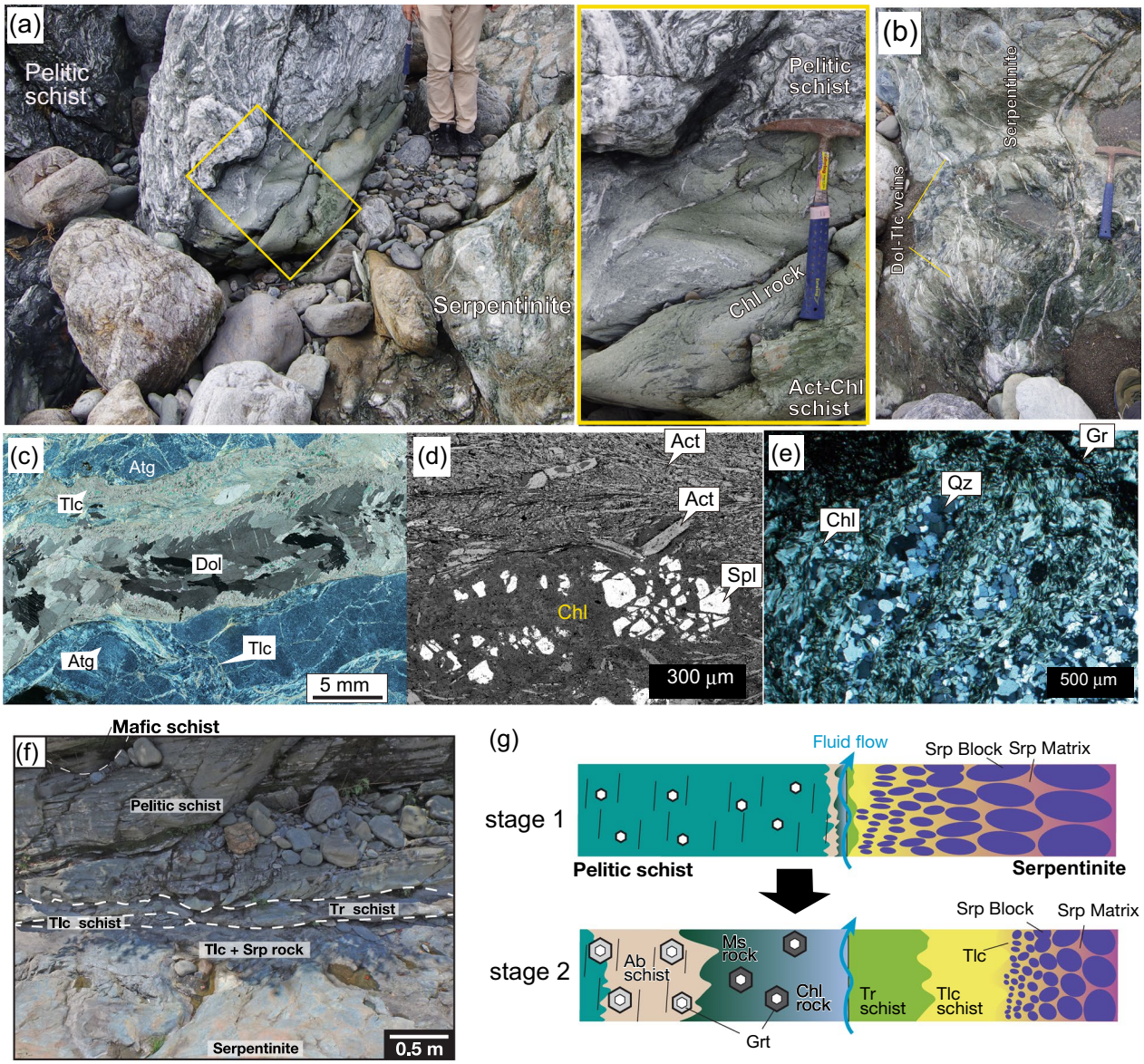

Fig. 4 **a**–**e** The Higuchi serpentinite body in the Sanbagawa belt, Japan (modified after Okamoto et al. 2021). **a**, left Outcrop photograph and (right) close-up view of the chlorite rock and the Act–Chl schist at the contact between a serpentinite body and pelitic schist. **b** Branching Tlc–Cb vein networks in the serpentinite body. **c** Photomicrograph of a dolomite vein with a talc selvage in the massive antigorite under cross-polarized light. **d** Back-scattered electron image of the Act–Chl schist. **e** Photomicrographs (plane-polarized light) of the chlorite rock, showing the relic banded graphite-rich layers and quartz veins in the pelitic schist. Chlorite has formed around the altered Cr-rich spinel. **f** Photograph and **g** sketch of the reaction zones between the serpentinite body and pelitic schist in Tomisato body (modified after Oyanagi et al. 2023). Act: actinolite, Chl: chlorite, Gr: graphite, Spl: spinel, Dol: dolomite, Tlc: talc, Qz: quartz, Grt: garnet, Atg: antigorite, Srp: serpentine

and K_2O, and grains in MgO, FeO, and H_2O, with near-constant TiO_2, P_2O_5, and Al_2O_3, resulting in ~ 30% solid volume decrease. This natural occurrence and mass balance analyses indicate the progress of chloritization by Mg-metasomatism in the pelitic schists (e.g., R4).

In summary, Mg-metasomatism occurred in the pelitic schist (crustal rocks) to form Chl rocks, and CO_2-metasomatism occurred in the serpentinite to form Mgs + Tlc and Dol + Tlc veins with intense fracturing. In this outcrop, the extent of Si-metasomatism in the serpentinite is not clear due to the heterogeneous occurrence of Tlc–Cb veins.

3.1.2 Tomisato serpentinite body

Another distinct crust–mantle contact is found in the Tomisato serpentinite body in central Shikoku. This body is also composed of massive antigorite serpentinite, and is cut by talc veins that developed in the marginal part of the body in contact with a pelitic schist, and tremolite veins that developed at the contact with a mafic schist (Hirauchi et al. 2021; Oyanagi et al. 2023). Oyanagi et al. (2023) showed that reaction zones developed along the contact between the pelitic schist and serpentinite, with the rock changing from pelitic schist to albite (Ab) schist, muscovite (Ms) rock, Chl rock, Tr–Chl schist, Tlc schist, and serpentinite (Fig. 4f). No carbonates occur in the reaction zones. The original boundary between the pelitic schists and serpentinite was located at the boundary between the Chl rock and Tr-Chl schists (Fig. 4g). The detailed mass balance calculations revealed a flux in SiO_2 with the minor transport of Al_2O_3 and CaO from the pelitic schist to serpentinite, and a flux of MgO from the serpentinite to the pelitic schist. The mass of Ca released from the pelitic schist and added to the serpentinite is not balanced, suggesting Ca is sourced from an external system.

In summary, the Tomisato serpentinite body is a representative natural example of bi-directional metasomatism: Mg-metasomatism of a pelitic schist to form Chl rock and Si–Ca–Al-metasomatism of serpentinite to form Tr–Chl and Tlc schists.

3.2 Serpentine shear zone along the Livingstone fault

The Livingstone fault in New Zealand is a serpentine shear zone that separates the ultramafic rocks of the Dun Mountain Ophiolite Belt from the metasedimentary and metavolcanic rocks of the continental Caples and Aspiring terranes (Tarling et al. 2019a). The Livingstone fault is composed of a wide zone of foliated serpentinite (up to ~ 480 m) that contains various blocks of crustal rocks, including metasedimentary, metabasaltic, and meta-ultramafic rocks (Fig. 5a, b; Tarling et al. 2019b). The serpentine minerals in the shear zone matrix are chrysotile and lizardite, suggesting temperatures lower than ~ 350 °C. Metasomatic reactions took place along the main shear zone boundaries, as well as at the contact between the crustal rocks and the serpentine matrix. Metasomatic alteration of the serpentinite to form Tr and Tlc veins and minor diopside occurred where it is

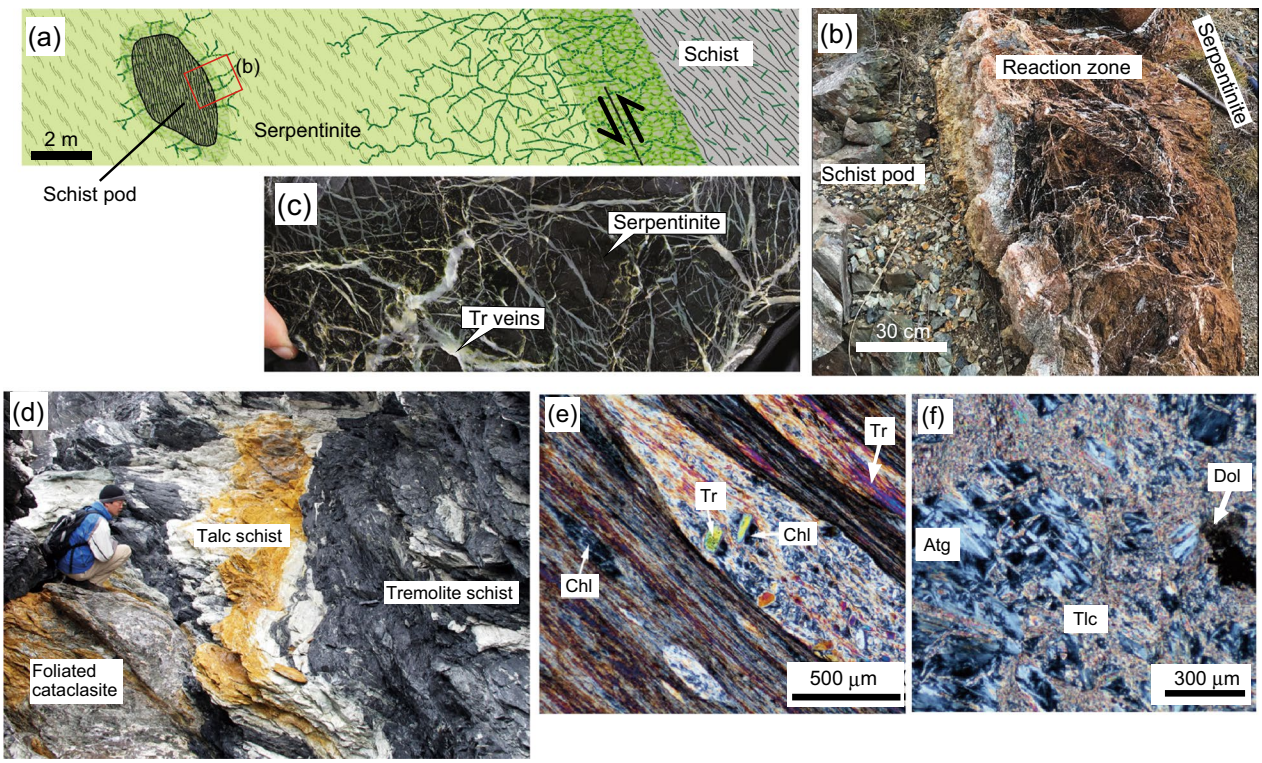

Fig. 5 **a**–**c** Livingstone fault in New Zealand (modified after Tarling et al. 2019b). **a** Schematic cross-section of metasomatic reaction zones adjacent to schist pods and serpentinites. **b** Outcrop of the reaction zone at the contact between schist and serpentinite. **c** Tremolite vein network that developed in the serpentinites. **d**–**f** Franciscan Complex in USA (modified after Hirauchi et al. 2020). **d** Photograph of the reaction zones at the contact between serpentinite and metasediment. **e**, **f** Photomicrographs of (**e**) talc networks in the serpentinite and (**f**) tremolite + chlorite rocks replacing the metasediments under cross-polarized light. Tr: tremolite, Chl: chlorite, Atg: antigorite, Tlc: talc, Dol: dolomite

in contact with crustal blocks (Fig. 5b, c; Tarling et al. 2019a, b). Tremolite is dominant, forming intense vein networks (Fig. 5c) or occurring as randomly oriented crystals replacing serpentinite, and the Tr-rich region is up to several meters thick (Fig. 5b). These metasomatic replacement textures and branching tensile veins are repeatedly cut by shear veins. These outcrops and Sr isotopic data suggest that the Si- and Ca-metasomatism in the serpentinites occurred as a result of the reaction with aqueous fluids that had reacted with the metasedimentary rocks. In contrast, there is no distinct evidence for Mg-metasomatism in the crustal rocks of this outcrop (Tarling et al. 2019a, b).

3.3 Metasediment–serpentinite contact in the Franciscan complex

A tectonic mélange in the Franciscan complex at Jade Cove, California, USA, contains the contact between metasediment and serpentinite (King et al. 2003; Hirauchi et al. 2020; Nagaya et al. 2020). The peak metamorphic conditions for the mélange matrix (metasediments) are estimated to be 150–200 °C and 0.4–0.6 GPa, and the serpentine records multiple serpentinization events, including the transition from lizardite and chrysotile to antigorite that occurs at ~ 250–300 °C (Schwarz et al. 2013). The composition of spinel in the serpentinite suggests that the serpentinite originated from the oceanic lithosphere (Hirauchi et al. 2008). The serpentinite bodies in the areas are interpreted to be oceanic mantle rocks that were subducted, exhumed, and incorporated into the Franciscan Complex.

The Jade Cove mélange exhibits metasomatism along the metasediment–serpentinite contacts (Fig. 5d). With increasing distance from the metasediment–serpentinite contact, the metasomatic zones in the serpentinite change from Tr–Chl rock (Fig. 5e) to Tlc–Chl rock (Fig. 5f), fully serpentinized peridotite, and partially serpentinized peridotite (King et al. 2003). The Tlc–Chl rocks are < 2 m thick (Hirauchi et al. 2020). The main phase of metasomatism of the serpentinite is thought to have occurred prior to its emplacement in the Franciscan Complex. The fractionation of O isotopes between silicate minerals suggests a temperature of 450–500 °C (Fig. 3; King et al. 2003). Mass balance calculations for the metasomatic zones in the serpentinite suggest that these reaction zones were formed by the addition of SiO_2 and CaO (King et al. 2003). The metasedimentary rocks adjacent to the serpentinite are metasomatized, characterized by the overgrowth of tremolite and minor chlorite along the pre-existing foliation of the metasedimentary rocks (Fig. 5e; Hirauchi et al. 2020). In summary, Si-metasomatism occurred in the serpentinite (Fig. 5f). Mg- and Ca-metasomatism occurred in the metasediments (Fig. 5e), but, as the temperatures estimated in serpentinite and metasediments are different (Fig. 3), the detail relationship between the metasomatism in serpentinite and in metasediments are not clear.

3.4 Metagabbro–serpentinite interface in the Voltri Massif

In the Voltri Massif of the Ligurian Alps in Italy, a metasomatic reaction zone developed between eclogitic metagabbro and serpentinite (Scambelluri and Rampone 1999; Codillo et al. 2022a). The geochemical characteristics indicate that the partial serpentinization occurred in an oceanic setting with subsequent modification during high pressure metamorphism in the subduction zone. The metagabbro does not contain quartz but consists of Cpx + garnet (Grt) + amphibole (Amp) + Ab + Fe-Ti oxides. The reaction zones are asymmetric and developed with a thickness of over ~ 1 m, mainly in the metagabbro. From the serpentinite (Zone I), the reaction zones consist of Ca-Amp ± Chl (Zone II), Chl + Ca-Amp (Zone III), and epidote (Zone IV; Fig. 6a). In contrast, a distinct metasomatic reaction zone did not form in the serpentinite, although a small amount of talc formed. The bulk-rock chemistry across the boundary has a diffusive profile, with Mg, Ni, and Cr contents decreasing from the serpentinite to the metagabbro (Fig. 6b). The bulk rock SiO_2 content of the serpentinite (~ 48–50 wt%) is higher than that of the metagabbro (40–43 wt%), with high Si contents in the amphibole-rich rock and low Si contents in the Chl rock near the contact (Fig. 6b). CaO contents are high in the metagabbro, but they decrease near the contact with the serpentinite. The stepwise pattern in the $^{87}Sr/^{86}Sr$ ratio and the trends in fluid-immobile elements indicate that the reaction zone developed through fluid-mediated metasomatic reactions rather than mechanical mixing (Codillo et al. 2022a).

Mass-balance calculations suggest that the formation of Chl-rich rocks at the expense of metagabbro (Zone III) requires the addition of Mg (~ 84 kg/m^2) and H_2O (~ 40 kg/m^2) as well as the removal of Ca (~ 10 kg/m^2) (Codillo et al. 2022a). The Ca removed during the formation of the Chl-rich rocks is redistributed to form Ca-amphibole and epidote in zones II and IV. In contrast, Si and Al contents remain almost constant. In summary, close to uni-directional metasomatism occurred at the contact between eclogitic metagabbro and serpentinite in the Voltri Massif, where significant Mg-metasomatism of the crustal rock occurred, with a smaller amount of Si-metasomatism occurring in the serpentinite. Similar asymmetric Mg-metasomatic reaction zones in mafic rock (blueschist) has been reported at a blueschist–serpentinite contact in high-*P* metamorphic rocks from Syros, Greece (Miller et al. 2009; Fig. 3).

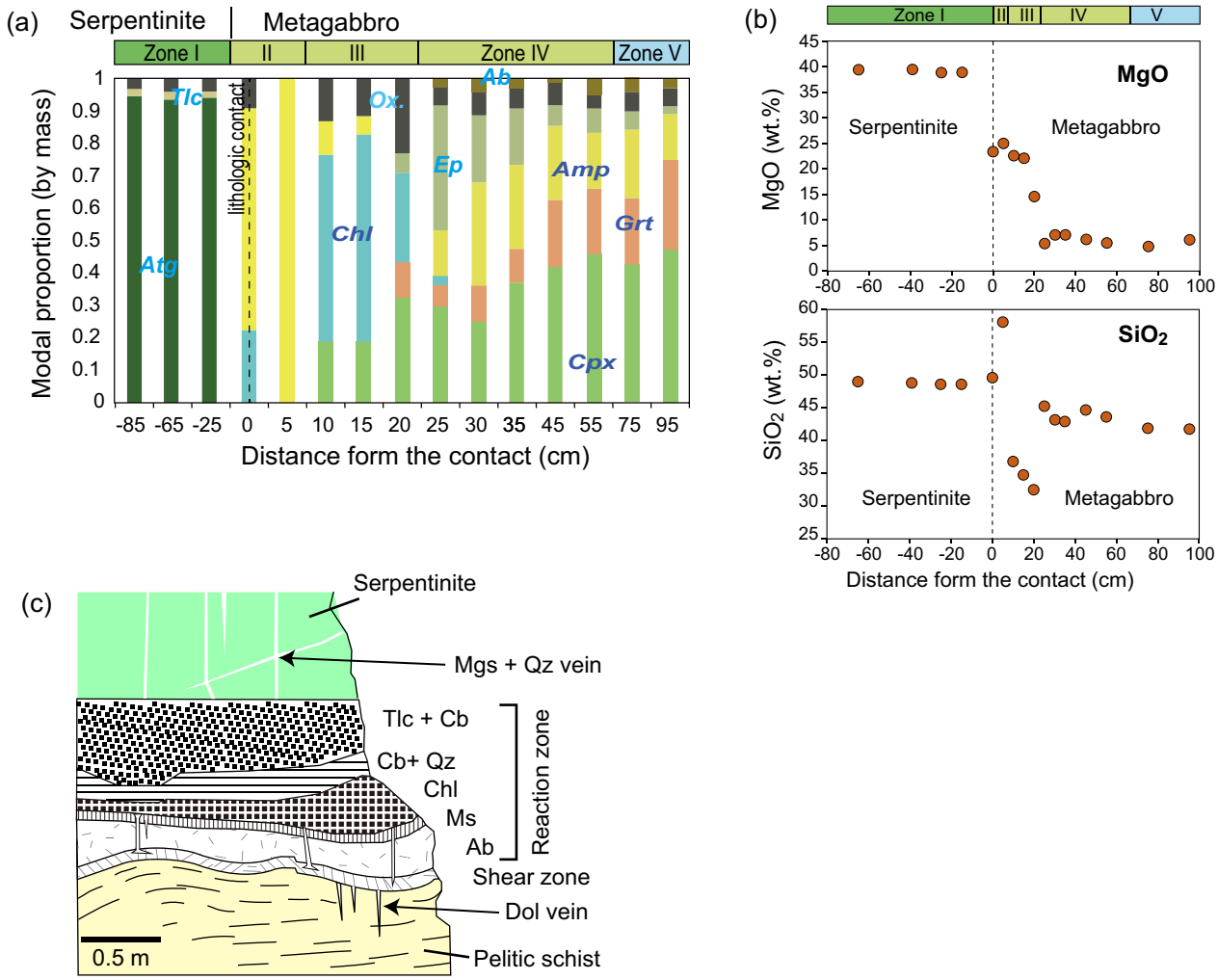

Fig. 6 **a**, **b** Reaction zones between a metagabbro and serpentinite in the Voltri Massif (modified after Codillo et al. 2022a). **a** Modal abundances of minerals in each zone. Zone I and Zone V represent the unaltered serpentinite and metagabbro, respectively. Zones II–IV are the reaction zone in the metagabbro. **b** Bulk rock composition as a function of distance from the metagabbro–serpentinite contact. Top panel: MgO, bottom panel: SiO_2. **c** Reaction zones between a pelitic schist and serpentinite in the Nishisonogi metamorphic rocks (modified after Mori et al. 2007). **c** Sketch of the reaction zones. Atg: antigorite, Chl: chlorite, Tlc: talc, Ep: epidote, Amp: amphibole, Grt: garnet, Cpx: clinopyroxene, Ab: albite, Ox: oxide, Cb: carbonate, Qz: quartz, Ms: muscovite

3.5 Serpentinite in Nishisonogi metamorphic rocks

The Nishisonogi metamorphic rocks in Kyushu, Japan, are part of a Late Cretaceous subduction complex (Mori et al. 2007). They consist mainly of pelitic, psammitic, and mafic schists with a small amount of serpentinite. Reaction zones (0.5–10.0 m thick) occur between the serpentinite and pelitic schist. The reaction zones are composed of monomineralic or bimineralic layers of Tlc + Cb, Act (or Cb + Qz), Chl, Ms, and Ab, in order from the serpentinite to the pelitic schist (Fig. 6c). Based on a discontinuity in the Ti content of the altered rocks, the original contact between the serpentinite and pelitic schist was identified at the boundary between the Act and Chl layers. Assuming that Ti is immobile, mass balance analyses show that the formation of the Tlc + Cb layer and Cb + Qz from serpentinite involved a gain of C and losses of CaO, MgO, and H_2O with little change in SiO_2. In contrast, the formation of the Chl, Ms, and Ab layers from the pelitic schist was characterized by gains in MgO, FeO, and H_2O, and losses of SiO_2, K_2O, and C, with little change in Al_2O_3. A gain in Na_2O is only found in the Ab layer. During the development of the reaction zone, the Tlc + Cb, Chl, and Ms layers decreased in solid volume by ~ 30%, and the Cb + Qz and Ab layers decreased in solid volume by ~ 10%. Fluid inclusion studies and Cal–Dol thermometry suggest that the veins

formed at > 350 °C at > 0.4 GPa (Mori et al. 2007, 2014). The immobility of SiO_2 in the Tlc + Cb and Qz + Cb zones suggests that this alteration of serpentinite is not Si-metasomatism. Alternatively, the carbonation of serpentinite formed magnesite or dolomite. The typical reactions of carbonation of serpentinite are the formation of Mgs + Tlc (R3) and Mgs + Qz.

$$\underset{\text{Serpentine}}{Mg_3Si_2O_5(OH)_4} + 3CO_2(aq) \rightarrow \underset{\text{Magnesite}}{3MgCO_3} + \underset{\text{Quartz}}{2SiO_2} + 2H_2O \quad \text{(R14)}$$

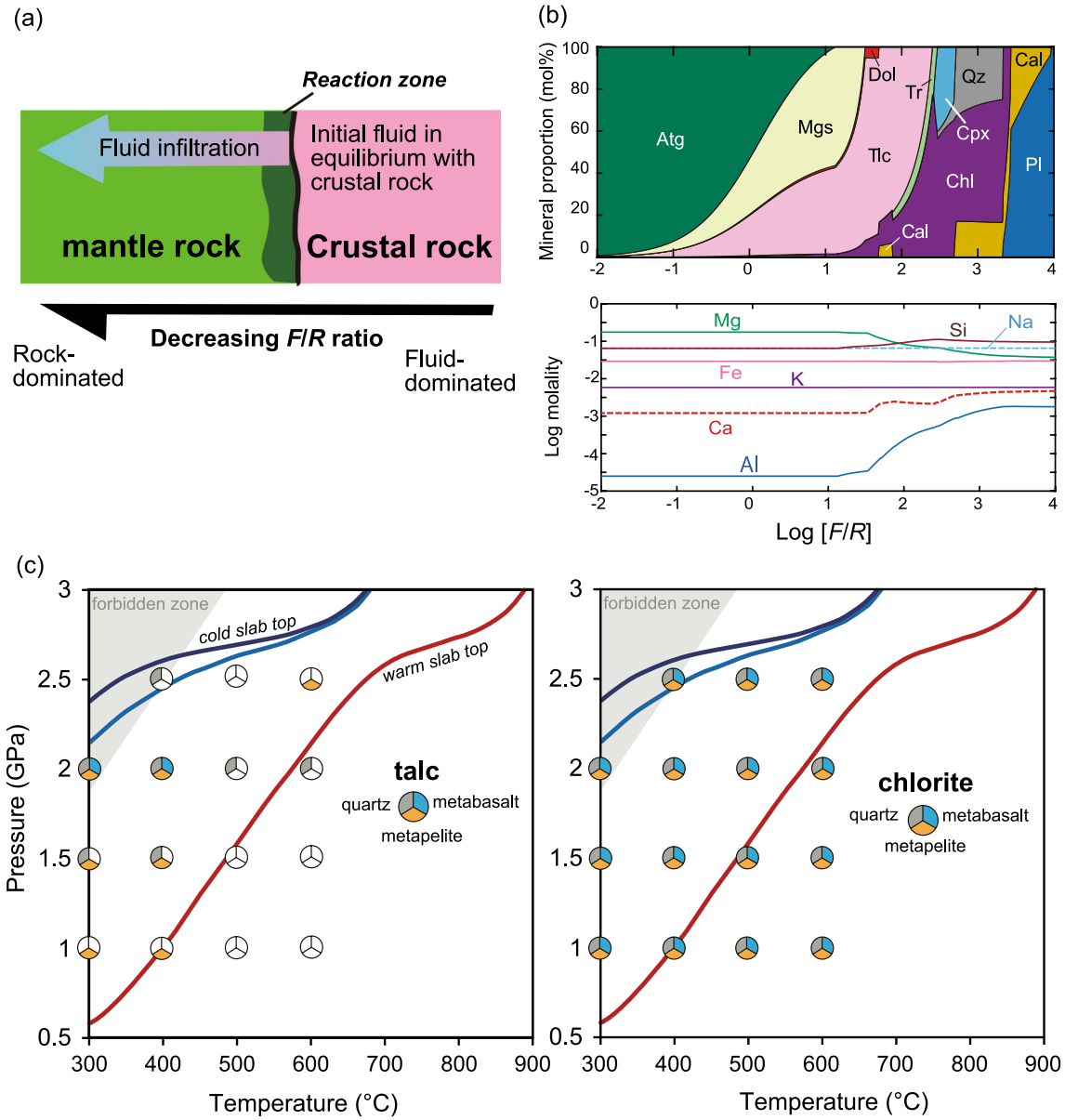

Fig. 7 **a** Schematic illustration of the fluid-to-rock (*F*/*R*) ratio in geochemical models of reaction zones between mantle and crustal rocks. A decrease in the *F*/*R* ratio indicates increasing infiltration of fluid in equilibrium with crustal rocks into the interior of the mantle rock. **b** Thermodynamic model of the interaction between pelitic schist-derived fluid and antigorite at 400 °C and 0.5 GPa. Stable mineral assemblage (top panel) and total concentration (mol/kg) of Si, Mg, Al, Na, K, Fe, and Ca in fluids (bottom panel) as a function of log(*F*/*R*) (modified after Okamoto et al. 2021). **c** Results of reaction path modeling on the stability of talc (left panel) and chlorite (right panel) during the interaction between mantle peridotite and fluids in equilibrium with crustal rocks (quartz, metabasalt, and metapelite; Codillo et al. 2022b). Atg: antigorite, Chl: chlorite, Tlc: talc, Tr: tremolite, Cpx: clinopyroxene, Pl: plagioclase, Mgs: magnesite, Dol: dolomite, Cal: calcite, Qz: quartz

The Mg-metasomatism of crustal rock also occurs through the transport of Mg from serpentinite to pelitic schist. Si transport from the crust to the mantle may have been inhibited by CO_2-metasomatism, as silica-rich minerals (quartz or talc) formed in serpentinite (R3, R14), which may have lowered the Si activity gradient across the crust–mantle contact.

4 Geochemical modeling of the slab–mantle interface in a subduction zone

4.1 Geochemical models of metasomatic processes

Metasomatic reactions involve rocks and fluids in multicomponent systems. Reaction path modeling is a powerful tool for predicting the products of metasomatic reactions using thermodynamic equilibrium in both minerals and aqueous species (e.g., Reed 1982; Bach and Klein 2009). To simulate the metasomatic reactions caused by fluid infiltration, two calculation steps are usually conducted. For example, when we model the infiltration of slab-derived fluids into mantle rocks, the composition of the fluid in equilibrium with crustal rocks is calculated initially, then mantle blocks are added incrementally to the fluids, and the equilibrium fluid composition and stable mineral assemblage are calculated. In this modeling, the fluid-to-rock mass (F/R) ratio represents the progress of the water–rock interaction (alteration and metasomatic reactions). A decrease in the F/R ratio in this model reflects the evolution of the local fluid–rock equilibrium as the fluid travels from the crustal rock into the mantle rock (Fig. 7a).

4.2 Modeling the metasomatism of ultramafic rocks by slab-derived fluids

To understand the metasomatic reactions between serpentinite and pelitic schist, Okamoto et al. (2021) conducted reaction path modeling at 400 °C and 0.5 and 1.0 GPa, in which antigorite blocks were incrementally added to fluids that were in equilibrium with graphite-bearing metapelite over a wide range of F/R ratios. When the input fluid equilibrated with the pelitic schist had a fO_2 close to the quartz–fayalite–magnetite buffer, the mineral sequence at the serpentinite–pelitic schist contact in the carbonated serpentinite (from Chl to Act + Chl, Cal + Dol, Dol + Tlc, Mgs + Tlc, and Atg) matched that observed in the Higuchi serpentinite body in the Sanbagawa belt (Fig. 7b). The highest concentration of Si in aqueous fluids occurs at high F/R ratios (near initial pelitic derived fluid), whereas at low F/R ratios (i.e., the interior of the serpentinite body), the total dissolved Mg content of the aqueous species is higher than the dissolved Si content (Fig. 7b). This is consistent with the large Mg flux into pelitic schist during the formation of chlorite rock (Mori et al. 2007; Okamoto et al. 2021; Oyanagi et al. 2023; Figs. 4, 6). At low F/R ratios, dehydration of serpentinite occurs during carbonation or Si metasomatism. This reaction path modeling reveals that the solid volume decreases during the carbonation and Si-metasomatism of serpentinite due to the outflux of Mg and H_2O (Okamoto et al. 2021). In contrast, the total volume (including the fluid volume) increases during metasomatic reactions. Even when the initial fluids had low fO_2 and carbonate was unstable, the trend is similar: the pelite-derived fluids are Si-rich, and fluids in regions of low F/R ratio (mantle rock-dominated) are Mg-rich (Okamoto et al. 2021).

Extensive reaction path modeling was conducted by Codillo et al. (2022b), in which ultramafic rocks (depleted mantle and harzburgite) were incrementally added to aqueous fluids in equilibrium with crustal minerals and rocks (quartz, metabasalt, and metasediment) over a wide range of P–T conditions (1.0–2.5 GPa, 300–600 °C; Fig. 7c). At constant pressure, the concentrations of dissolved Al and Si in fluids in equilibrium with the metapelite increase with increasing temperature, whereas the concentration of dissolved Mg is predicted to decrease as the temperature increases from 300 to 400 °C, and then slightly to increase from 500 to 600 °C. The appearance of talc and chlorite in the products of the fluid–rock interaction depends on the P–T conditions and the type of slab-derived fluid (Fig. 7c; Codillo et al. 2022b). Talc forms on the geotherm only in cold subduction zones, and it forms preferentially through metasomatic reactions with quartz or metapelite rather than those with metabasalt. In contrast, chlorite forms under all P–T conditions and for all types of fluid. Based on these results, Codillo et al. (2022b) proposed that talc formation in a subduction zone is less common than chlorite formation, except for in cold subduction zones. The formation of chlorite results from the dissolved Al in the slab-derived fluids. For example, when Si is assumed to be fixed, chlorite formation from serpentinite can be expressed as follows.

$$\underset{\text{Serpentine}}{3Mg_3Si_2O_5(OH)_4} + 2Al_2O_3(aq) + MgO(aq) + 2\,H_2O \rightarrow \underset{\text{Chlorite}}{2Mg_5Al_2Si_3O_{10}(OH)_8} \quad \text{(R15)}$$

In warm subduction zones (e.g., the Tomisato serpentinite; Fig. 3), a small amount of chlorite forms in serpentinite in response to the Al flux from the pelitic schist (Oyanagi et al. 2023), but the main metasomatic minerals in the serpentinite are tremolite and talc. The discrepancy between the model (Codillo et al. 2022b)

and natural samples may be caused by external chemical flux (e.g., Ca) via fluid flow along lithological boundaries (Fig. 4d), and by the different bulk compositions of serpentinite (Oyanagi et al. 2023).

4.3 Incremental addition of metagabbro to serpentine-buffered fluids

Eclogitic metagabbro from the Voltri Massif does not contain quartz, and a reaction zone has developed in the metagabbro at the contact with serpentinite (Codillo et al. 2022a). Codillo et al. (2022a) conducted geochemical modeling in which metagabbro (anorthite (An) + diopside (Di)) was incrementally added to fluids in equilibrium with serpentinite (Atg + Di + Mag ± Brc). The serpentinite-buffered fluid is dominated by dissolved Mg and Si, with the contents of dissolved Ca and Al being several orders of magnitude lower. $Mg(OH)_{2(aq)}$ is the most dominant species in the fluid. With decreasing *F/R* ratios, the mineral assemblage changes from Atg + Cpx to Atg + Cpx + Chl, Chl + Cpx ± Tr, and Grt + Chl + Cpx + epidote (Ep) + paragonite (Pa) ± Pl ± Qz. Chlorite forms in the altered metagabbro mainly at intermediate *F/R* ratios (10^0–10^3), and dissolved Al concentrations are elevated at *F/R* ratios of 10^0–10^1. The dominant formation of chlorite at intermediate *F/R* ratios is consistent with the variation in the reaction zones in the eclogitic metagabbro with distance from the contact with the serpentinite in the Voltri Massif (Fig. 5a; Codillo et al. 2022a).

5 Discussion

5.1 Relative mobility of Mg and Si in subduction zones

5.1.1 Variations in metasomatic reaction zones at the crust–mantle interface

The results of hydrothermal experiments using Ol–Qz and Ol–Pl systems, that talc or Al-rich serpentine form preferentially in the Ol-hosted region (Fig. 2b, c; Oyanagi et al. 2015, 2018, 2020), show that Si is transported mainly from crust to mantle, whereas Mg is relatively immobile. The development of the Si-metasomatic reaction zones in mantle rocks is consistent with the considerable formation of talc rock in ultramafic rocks exposed on the ocean floor (e.g., Bach et al. 2006; Boschi et al. 2006; Schwarzenbach et al. 2021) and the reaction zones in serpentine shear zones along contacts with metapelites at relatively low temperatures (Figs. 3, 4a–c; Tarling et al. 2019a).

In contrast, exposed crust–mantle contacts in high-pressure metamorphic rocks suggest distinct bi-directional metasomatism: Si-metasomatism of serpentinites to form talc, and Mg-metasomatism of metapelite to form chlorite (Fig. 4; Okamoto et al. 2021; Hoover et al. 2022; Oyanagi et al. 2023). Asymmetric reaction zones have been reported along the contact between serpentinite and metagabbro or metabasaltic rocks, where Mg-metasomatism occurred in the crustal rocks, but there was a lack of Si-metasomatism of mantle rocks (Fig. 5; Mori et al. 2014; Codillo et al. 2022a). The variations in reaction zones between crustal and mantle rocks suggest that the relative mobility of Mg from mantle to crust and Si from crust to mantle can vary in response to the geological setting. What factors control the relative mobilities of Si and Mg in laboratory experiments and natural settings?

For chemical transport involving fluid-mediated reactions, two transport mechanisms are possible: diffusion in fluids and fluid advection. In batch experiments on analogue to crust–mantle contacts, fluid advection was not involved in the metasomatic reactions (Ogasawara et al. 2013; Oyanagi et al. 2015, 2018, 2020). These experiments are similar to the simple bi-metasomatic reactive diffusion model (Frantz and Mao 1979; Lichtner et al. 1986). In subduction zones, chemical transport could occur via fluid advection, as fluid is commonly generated by dehydration of the subducting sediments or hydrated oceanic crust (e.g., Okamoto et al. 2017; Taetz et al. 2018). However, Mg, Ni, and Cr profiles in metagabbro from the contact with serpentinite indicate the predominance of diffusive elemental transport from mantle to crust (Codillo et al. 2022b). A large difference in aqueous diffusion coefficients for Mg and Si species is not expected in aqueous fluids (Oelkers and Helgeson, 1988). Instead, it is reasonable to consider that the difference in reaction zones is essentially controlled by the concentration gradients of dissolved Mg and Si in the fluid.

As shown above, reaction path modeling can simulate local compositional changes in fluids as they pass through the rocks (e.g., Bach and Klein 2009; Okamoto et al. 2021; Codillo et al. 2022a, b). Recent geochemical modeling suggests that the dissolved Mg content in fluids buffered by mantle rocks is several orders of magnitude higher than that in fluids buffered by quartz-bearing crustal rocks, which may facilitate a significant flux of Mg from mantle to crust (Okamoto et al. 2021; Codillo et al. 2022a, b). Based on models of the incremental addition of mantle rocks to crustal-rock-buffered fluids, Codillo et al. (2022b) proposed that chlorite forms (R15) preferentially over talc in the serpentinite under a wide range of *P*–*T* conditions (Fig. 3). However, there are no studies that compare the flux of Si from mantle to crust with that of Mg from mantle to crust systematically.

5.1.2 Dissolved Si in pelite-derived fluids versus Mg in mantle-derived fluids

To understand the relative mobilities of Mg and Si, we calculated fluid compositions in equilibrium with mantle

peridotite and pelite. Thermodynamic modeling of fluid and rock in the Na–K–Ca–Fe–Mg–Al–Si–C–O–H system was conducted using the DEW model (Sverjensky et al. 2014; Huang and Sverjensky 2019) implemented in Perple_X version 7.0.2 (Connolly 2005). See Supporting Information for detail. For selected *P*–*T* conditions, metasomatism induced by fluid infiltration was also modeled by the 0-dimensional infiltration model in the Perple_X version 7.0.2. In the model, mineral equilibria were computed by incremental addition of a fluid to a rock mass (e.g., Connolly and Galvez 2018; Menzel et al. 2020; Muñoz-Montecinos et al. 2021).

The geochemical calculations were conducted using the geotherm along the slab top calculated by van Keken et al. (2018) for the NE Japan, Nankai, and Cascadia subduction zones (Fig. 3), and pressures of 0.2–2.5 GPa. NE Japan is a cold subduction zone, whereas the latter two are warm subduction zones; e.g., the slab top temperatures at 1.0 GPa are 230 °C in NE Japan, 468 °C in Nankai, and 519 °C in Cascadia (Fig. 3). Figure 8a–c shows the calculated dissolved Si, Al, Mg, and Ca contents and Δ pH ($pH - pH_{Neutral}$) in the fluid in equilibrium with pelitic schist (i.e., pelite-derived fluids) in the NE Japan (Fig. 8a), Nankai (Fig. 8b), and Cascadia (Fig. 8c) subduction zones. Figure 8d–f shows the results for fluid in equilibrium with peridotite (i.e., mantle-derived fluids) in the NE Japan (Fig. 8d), Nankai (Fig. 8e), and Cascadia (Fig. 8f) subduction zones. The speciation of Mg, Si, Ca, and Al in the fluids is also shown for pelite-derived (Fig. 9a–c) and mantle-derived (Fig. 9d–f) fluids, respectively. The mineral assemblage in each rock varies with increasing depth, and the mantle rock is extensively serpentinized (Additional file 1: Fig. S1).

In the NE Japan (Fig. 8a) and Nankai (Fig. 8b) subduction zones, the pelite-derived fluid is alkaline (ΔpH > 0), with Δ pH decreasing with depth from ~ 3.5 to ~ 1.5. In the Cascadia subduction zone, the Δ pH is nearly constant (1.5–2.0) (Fig. 8c). The concentration of dissolved Si (total for all Si-bearing species) in the pelite-derived fluids is higher than the concentrations of other elements (e.g., Mg, Ca, Al) in all subduction zones, and the Si concentration increases with depth (Fig. 8a–c). The dissolved Mg, Ca, and Al concentrations increase sharply with pressure at shallow depths, but their contents increase

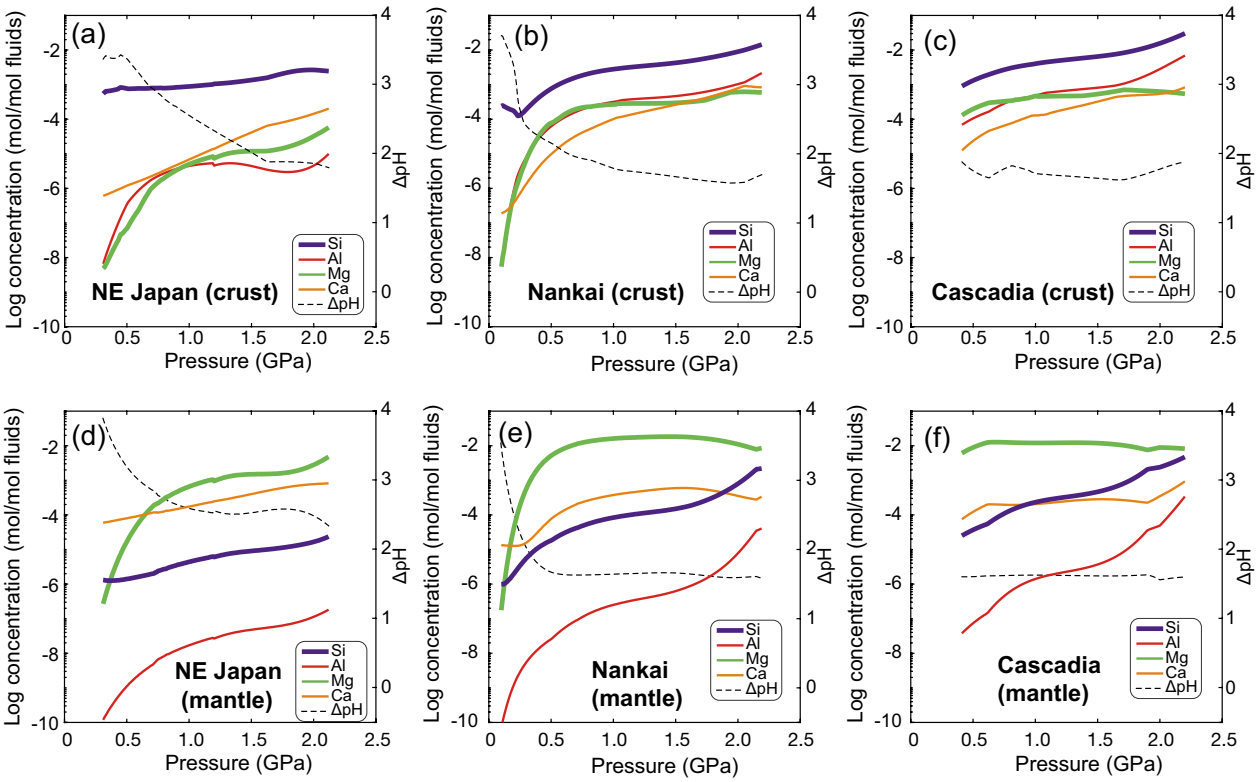

Fig. 8 **a**–**c** Total concentrations of dissolved Si (C_{Si}), Mg (C_{Mg}), Al (C_{Al}), and Ca (C_{Ca}) in the fluid in equilibrium with pelitic schist (crust) for the *P*–*T* conditions along the upper surface of the slab in the **a** NE Japan, **b** Nankai, and **c** Cascadia subduction zones. **d**–**f** Total concentrations of dissolved Si (C_{Si}), Mg (C_{Mg}), Al (C_{Al}), and Ca (C_{Ca}) in fluid in equilibrium with peridotite (mantle) for the *P*–*T* conditions along the upper surface of the slab in the **d** NE Japan, **e** Nankai, and **f** Cascadia subduction zones. ΔpH = pH – pH(neutral) at each *P*–*T* condition. The *P*–*T* paths along the upper surface of the slab in the NE Japan, Nankai, and Cascadia subduction zones are from van Keken et al. (2018; Fig. 3)

more slowly at depth. The differences between the dissolved Si content and the contents of the other elements are largest in the NE Japan (Fig. 8a). The most abundant Si species in NE Japan is $NaHSiO_3^-$, whereas it is $SiO_{2(aq)}$ in Nankai and Cascadia (Fig. 9a–c). In all three subduction zones, the most abundant species of Mg and Ca are $MgO_{(aq)}$ and $Ca(HCO_3)^-$, respectively. The Al species exist as Al-Si complex ($AlO_2(SiO_2)^-$).

For the mantle-derived fluids, ΔpH in NE Japan (~2.5 at 1.0–2.0 GPa; Fig. 8d) is higher than that in the other two subduction zones (~1.7 at 1.0–2.0 GPa; Fig. 8e, f). In contrast to the pelite-derived fluids, the dissolved Mg contents are generally higher than the dissolved Si contents. In NE Japan and Nankai (Fig. 8d, e), the dissolved Mg content sharply increases with depth and exceeds the dissolved Si content at 0.4 and 0.2 GPa, respectively. The dissolved Si content is lower than the dissolved Ca content over most of the pressure range but is several orders of magnitude higher than the dissolved Al content. In Cascadia (Fig. 8f), the dissolved Mg content is highest at pressures of 0.5–2.0 GPa. The dissolved Si content in the mantle-derived fluids increases with increasing pressure. In all three subduction zones, $MgO_{(aq)}$ is the dominant Mg species (Fig. 9d–f). Both neutral ($SiO_{2(aq)}$) and ionic ($HSiO_3^-$) Si species are abundant in NE Japan (Fig. 9d), whereas $SiO_{2(aq)}$ is dominant in Nankai and Cascadia (Fig. 9e, f). $Ca(OH)^-$ is the dominant Ca species in NE Japan, whereas $CaO_{(aq)}$ is dominant in Nankai and Cascadia. Al is dominantly present as AlO_2^- or Al–Si complexes [$AlO_2(SiO_2)^-$].

For evaluating the relative mobility of Mg and Si, Fig. 10a shows the logarithm of the ratios of the dissolved Mg concentration in the mantle-derived fluid to the dissolved Si concentration in the pelite-derived fluid (log MS ratio). At shallow depths in NE Japan and Nankai, the log MS ratio is negative, meaning that the dissolved Si content in the pelite-derived fluid is much higher than the dissolved Mg content in the mantle-derived fluid. The negative log MS ratios at low pressures and temperatures represent high Si mobility from crust to mantle, which is consistent with hydrothermal experiments that show only Si is transported from crust to mantle (Oyanagi et al. 2015, 2018, 2020). The log MS ratio increases greatly with increasing depth (Fig. 8a). The log MS ratio exceeds zero at pressures of 1.2 GPa in NE Japan and at lower pressures (< 0.3 GPa) in Nankai and Cascadia. This trend is consistent with the increase in $MgO_{(aq)}$ content of the mantle-derived fluids (Fig. 7d–f). In regions where the log MS ratio is positive, the mobility of Mg from mantle to crust is greater than that of Si from crust to mantle.

Metasomatism of metasediment by fluids equilibrated with ultramafic rock and metasomatism of mantle rock by fluids equilibrated with metasediment were modeled at 1.0 GPa in the NE Japan (Fig. 10b, c) and Nankai, subduction zones (Fig. 10d, e), respectively. The results of metasomatism of metasediment at NE Japan show that even when 300 mol of mantle-derived fluid was infiltrated in the metasediments ($F/R = \sim 5$), the initial mineral assemblage of Ms + lawsonite (Lws) + clinopyroxene (Cpx) + Qz + stilpnomelane (Stp)) does not change significantly (Fig. 10b, left panel), and a small amount of chlorite forms. In the cases of the metasomatism of antigorite serpentinite by fluids equilibrated with metasediments, chlorite always exists even when no fluid is added (Fig. 10b, right panel). The formation of chlorite predicted by the model (Fig. 10b) is in apparent contradiction with natural serpentinites, where little chlorite formed (e.g., Shiraga, Tomisato, Jade Cove; Fig. 4; Okamoto et al. 2021; Oyanagi et al. 2023). This discrepancy is due to the high Al content of the initial ultramafic rock used in the model (harzburgite; $Al_2O_3 = 4.5$ wt%; Additional file 1: Table S1). As the amount of pelitic-derived fluid increases, talc is mainly formed at the expense of antigorite (Fig. 10b, right panel). Minor amphibole also appears at relatively low *F/R* ratios at the expense of Cpx, and aragonite appear at higher *F/R* ratios. During the fluid-rock interaction, the Si gain in mantle rock is slightly higher than the Mg gain in metapelite (Fig. 10c), which is consistent with the Log MS ratio is close to zero (point 1 at Fig. 10a).

In Nankai, the mineral assemblages undergo significant changes as the amount of fluid infiltrated increases. At 400 mol fluids added ($F/R = \sim 7$), the metapelite is almost completely replaced by Chl + Amp, and the amount of chlorite sharply increases with increasing the *F/R* ratio (Fig. 10d). The progress of talc formation after antigorite in Nankai proceeds much greater than NE Japan, and antigorite is completely consumed at $F/R = \sim 1.5$. Dolomite and magnesite appear in higher *F/R* ratio. The value of Si gain of the serpentinite in Nankai is similar to that in NE Japan, whereas the Mg gain of the metapelite is extremely higher in the Nankai compared to the NE Japan (Fig. 10e). This reflects the positive log MS ratio in Fig. 10a. The trends of mineralogy and mass changes of Cascadia (Additional file 1: Fig. S2) are similar to those of Nankai (Fig. 10d, e).

Si-metasomatism of mantle rocks (serpentinite) induced by slab-derived fluids is likely to occur in both cold (e.g., NE Japan) and warm (e.g., Nankai and Cascadia) subduction zones (Fig. 11). In contrast, Mg-metasomatism of crustal rocks may occur preferentially in warmer subduction zones. Our geochemical modeling shows that talc formation in serpentinite by Si-metasomatism proceeds further in warm subduction zones (Fig. 10d) than in cold subduction zones (Fig. 10b). The formation of talc predicted along warm geotherms (Fig. 10d) differs from the results of Codillo et al. (2022b)

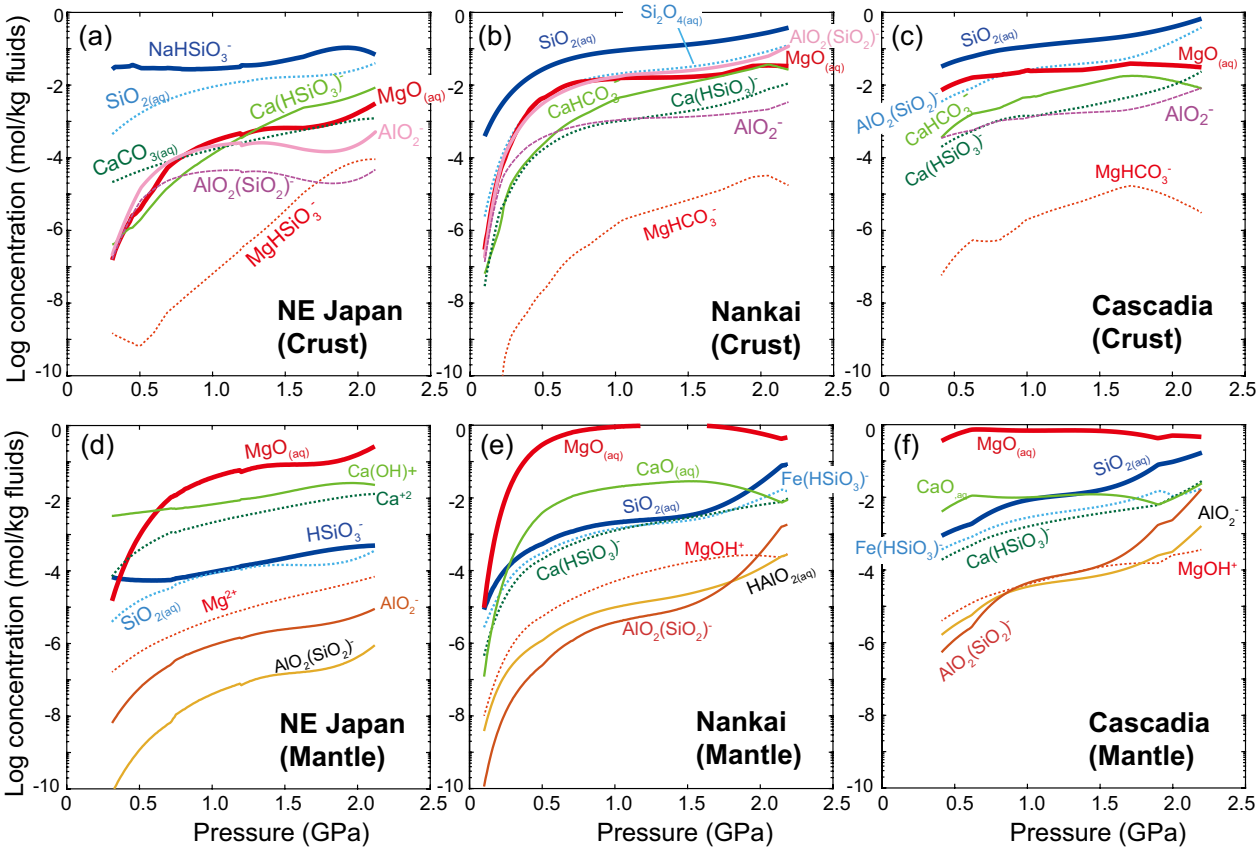

Fig. 9 Speciation of Mg, Si, Ca, and Al in aqueous fluids in **a**–**c** pelite-derived and **d**–**f** mantle-derived fluids calculated using geochemical models of the incremental addition of pelite and mantle peridotite (Fig. 8) in the **a**, **d** NE Japan, **b**, **e** Nankai, and **c**, **f** Cascadia subduction zones. For each element, the two most abundant species are shown

(Fig. 7b) but is consistent with the occurrence of talc in the Tomisato and Shiraga serpentinite bodies in the Sanbagawa belt (Fig. 4f, g; Kawahara et al. 2016; Oyanagi et al. 2023). The difference between the talc stability field calculated by Codillo et al. (2022b) (Fig. 7) and in this study (Fig. 10) may be due to the activity models for the Al-bearing minerals (e.g., chlorite, muscovite) used in the thermodynamic calculations. At large *F/R* ratios, aragonite occurs in altered serpentinite in NE Japan (Fig. 10b), and dolomite occurs at Nankai and Cascadia (Fig. 10d; Additional file 1: S2a). These calculated results for the warm subduction zones are consistent with the occurrences of carbonated mantle within subduction zone geotherms (e.g., Mori et al. 2007; Okamoto et al. 2021; Figs. 4b, c; 6c).

(See figure on next page.)

Fig. 10 **a** Logarithm of the ratio of the total dissolved Mg content in mantle-derived fluid [log C_{Mg} (mantle)] to the total dissolved Si content in metapelite-derived fluid [log C_{Si} (crust)] for the *P*–*T* conditions along the upper surface of the slab in the NE Japan, Nankai, and Cascadia subduction zones [log MS ratio = log C_{Mg} (mantle)/log C_{Si} (crust)]. Labels 1 and 2 indicate the *P*–*T* conditions for the thermodynamic calculation of fluid-rock interaction in (**b**–**c**). The *P*–*T* paths along the upper surface of the slab in the NE Japan, Nankai, and Cascadia subduction zones are from van Keken et al. (2018; Fig. 3). **b**–**e** Results of the thermodynamic calculations on the infiltration of fluids equilibrated with ultramafic rocks into metasediments (left panel) and on the infiltration of fluids equilibrated with metasediments into ultramafic rocks (right panel). **b** Mineral mode (%) and **c** mass change (g) of 1 kg protolith with respect to moles of fluid added to 1 kg rock in NE Japan (230 °C and 1.0GPa; point 1 in Fig. 10a). **d** Mineral mode (%) and **e** mass change (g) of 1 kg protolith with respect to moles of fluid added to 1 kg rock in Nankai (468 °C and 1.0GPa; point 2 in Fig. 10a). F/R ratio means the fluid-to-rock mass ratio. The results for Cascadia at the same pressure (519 °C and 1.0 GPa) are shown in Additional file 1: Fig. S2. For the F/R ratio labeled by "Not calculated", the thermodynamic calculations were failed due to the convergent problem. Arg: aragonite, Cpx: clinopyroxene, Ms: muscovite, Lws: lawsonite, Stp: stilpnomelane, Qz: quartz,Amp: amphibole, Chl: chlorite, Tlc: talc, Atg: antigorite, Ep: epidote, Ab: albite, Bt: biotite, Mgs: magnesite, Dol: dolomite

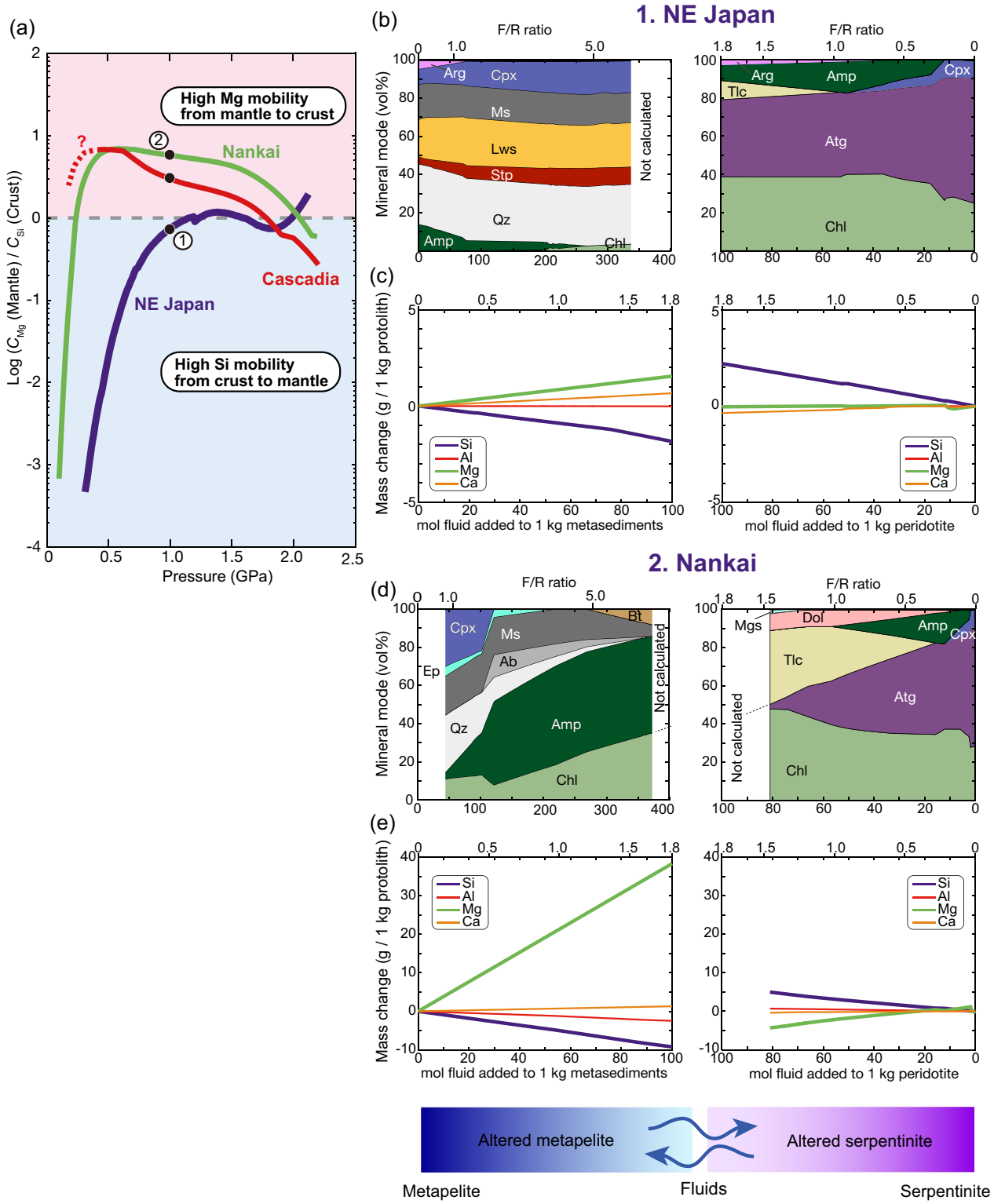

Fig. 10 (See legend on previous page.)

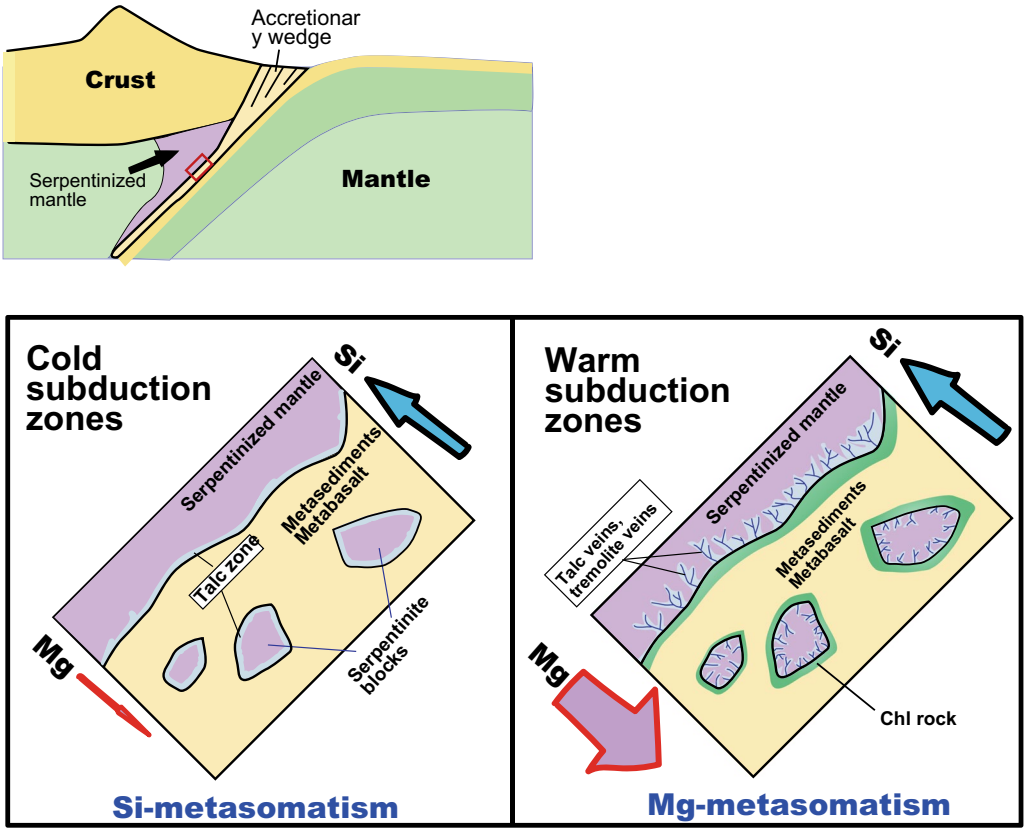

Fig. 11 Schematic illustration of Mg- and Si-metasomatism at the slab–mantle interface in a subduction zone (Top panel). In the cold subduction zones, Si is transported from crust to mantle to form the talc zone within the hydrated serpentinite (Bottom left panel). In the warm subduction zone, Mg is transported from mantle to crust to form chlorite rocks within the crustal rocks. Si-metasomatism also occurs occasionally to form talc and tremolite vein networks (Bottom right panel)

5.2 Formation of talc versus chlorite: the effect of Al mobility

Talc and chlorite are hydrous Mg–Fe silicate minerals that form during metasomatism between crust and mantle, but chlorite is characterized by high Al content. The progress of metamorphic reactions in high-grade metamorphic rocks is often controlled by the diffusion of Al (Miyazaki 2001). Hydrothermal experiments on the Ol–Pl interface show that migration of the Al-metasomatic front is slower than that of the Si-metasomatic front (Oyanagi et al. 2018; Fig. 2c).

In natural crust–mantle contacts in metamorphic terranes, talc commonly forms in metasomatized serpentinite (c.f. R1), whereas chlorite forms preferentially in metasomatized crustal rocks (c.f. R4; Mori et al. 2014; Okamoto et al. 2021; Codillo et al. 2022a; Oyanagi et al. 2023). Chlorite or Al-rich serpentine also forms in serpentinites (c.f. R14), but commonly close to Al-rich minerals, including Cr-spinel and Cpx (e.g., Okamoto et al. 2021). Al-rich minerals such as plagioclase and mica are abundant in crustal rocks (metasedimentary and metabasaltic rocks). Manning (2007) showed experimentally that the mobility of Al can be enhanced by the formation of Al–Si complexes, including $HAlSiO_{4,aq}$, at high temperatures and pressures. The importance of Al–Si complexes is predicted in the thermodynamic models (Fig. 9), although the detailed dependence of the Al–Si stoichiometry and the charge of the complexes on the pH and P–T conditions is still not fully understood. The geochemical modelling shown in this study (Figs. 8, 9, 10) predicts that the dissolved Al contents are more than two orders of magnitude lower than the dissolved Si contents in crust-derived fluids and dissolved Mg contents in mantle-derived fluids. As a result, Al is not immobile, but Al mobility is much lower than that of Si and Mg; therefore, the formation of asymmetric talc and chlorite zones is controlled by the distribution of Al-rich minerals in the protolith (Al-rich metapelite and metabasaltic rocks versus Al-poor serpentinites; Table 1), as observed in natural asymmetric metasomatic zones along contacts between serpentinite and metagabbro or pelitic schists (Figs. 4, 6). In summary, talc is commonly formed by the Si-metasomatism of mantle rocks (R1), whereas chlorite, not talc, is commonly formed by the Mg-metasomatism of crustal

rocks (R4; Figs. 9, 10; Table 1). It is noted that the other elements influence the fundamental trend of Mg- versus Si-metasomatism above as follows. Chlorite can form in Al-rich ultramafic rocks (Fig. 10b, d), and Ca contents in protoliths also strongly controls how much amphibole involves in the metasomatic products at the crust-mantle interface (Fig. 10b, d). The infiltration of CO_2-rich fluids also induces the formation of talc from mantle rocks even without the addition of Si or removal of Mg (R3, R14; e.g., Mori et al. 2007; Okamoto et al. 2021; Sieber et al. 2020; 2022; Figs. 2, 4b, c, 6c).

5.3 Solid volume change, water production, and reaction-induced fracturing

Metasomatic reactions involving significant chemical transport tend to cause a change in rock volume. In the diffusion–reaction model of Lichtner et al. (1986), the diffusive flux of Si is greater than that of Mg, and the solid volume of the talc zone increases in the Ol-hosted region and decreases in the Qz-hosted region (Fig. 1b). Similar solid volume changes have been observed at Ol–Qz and Ol–Pl contacts in hydrothermal experiments using mineral powders (Fig. 2b-g; Oyanagi et al. 2015, 2018, 2023). The initial ~ 37% porosity of Ol sand in the experiments was decreased to < 5% in the Tlc zone, resulting in a decrease in the effective diffusion coefficient (Oyanagi et al. 2020). As a result, in the experiments using mineral powders, the rate-limiting process of Si-metasomatism changes with the progress of metasomatic reactions from surface-controlled to diffusion-controlled (Oyanagi et al. 2020; Fig. 2f).

Natural rocks at the crust–mantle interface in subduction zones have much lower porosity than the porous media used in hydrothermal experiments, so an increase in solid volume during metasomatism cannot be accommodated easily to maintain fluid pathways. The formation of chlorite rocks in metapelites and metagabbros is commonly accompanied by a large reduction in solid volume (Mori et al. 2014; Okamoto et al. 2021; Codillo et al. 2022a; Oyanagi et al. 2023). For example, the formation of Chl rock from the pelitic schist at contact with serpentinite from the Sanbagawa belt shows a 30% decrease in solid volume (Okamoto et al. 2021). The Chl rock well preserves the original shapes of the banding and quartz grains in pelitic schist (Fig. 3e). Such pseudomorphic replacement reactions with large element transport could proceed pervasively by coupled dissolution and precipitation processes with the formation of transient porosity (e.g., Putnis et al. 2009; Plümper et al. 2017; Nurdiana et al. 2021). In contrast, Si-metasomatism in the serpentinite, including the formation of talc and tremolite, is often accompanied by the development of branching fracture networks (Figs. 3b, 4; e.g., Okamoto et al. 2021; Tarling et al. 2019b; Oyanagi et al. 2023). Reaction-induced fracturing also enhances chemical transport during metasomatic reactions (see below). Geochemical modeling of the incremental addition of antigorite to pelite-derived fluids (Okamoto et al. 2021) has shown that Si-metasomatism of a serpentinite body produces a decrease in solid volume, because dehydration occurs with Si- and CO_2-metasomatism and a large amount of Mg is transported from mantle to crust. This volume contraction is consistent with the results of the experiment on carbonation of serpentinite under the mantle wedge conditions (Sieber et al. 2020).

Hydration, dehydration, carbonation, decarbonation, and metasomatic reactions cause large changes in the solid volume. These solid volume-changing reactions often perturb the local stress field, resulting in reaction-induced fracturing (e.g., Jamtveit et al. 2000; Kelemen and Hirth 2012; Okamoto and Shimizu 2015). As a result, the feedback between mass transport, surface reaction, and fracturing plays an essential role in the progress of fluid-mediated solid volume-changing reactions. Numerical simulations using the distinct element method (DEM) provide insight into the feedback among fluid flow, surface reaction, and fracturing during solid volume-changing reactions. In the case of solid volume-decreasing dehydration reactions, the reaction proceeds with the release of fluids, and fine tensile fractures occur due to shrinkage, forming tree-like fracture networks (Malthe-Sørenssen et al. 2006; Okamoto and Shimizu 2015). In contrast, polygonal fractures, such as mesh textures, develop through hierarchical fracturing due to solid volume increase (Jamtveit et al. 2008; Okamoto and Shimizu 2015; Shimizu and Okamoto 2016), and this swelling is often accompanied by radial fracturing within the surrounding matrix, as observed in the fracturing of the plagioclase matrix adjacent to serpentinized olivine grains in troctolite (Kelemen and Hirth 2012; Jamtveit et al. 2008; Okamoto et al. 2017; Yoshida et al. 2020). Reaction-induced fracturing enhances the permeability of low-porosity rocks by several orders of magnitude, which plays an essential role in the pervasive serpentinization and carbonation of ultramafic bodies (e.g., Jamtiveit et al. 2008; Kelemen and Hirth 2012; Yoshida et al. 2020; Uno et al. 2022).

One of the common features in the natural metasomatic reaction zones at the crust-mantle interfaces is that fractures are preferentially developed in serpentinite (Fig. 2; Table 1). In the case of the crust–mantle interface in a subduction zone, branching fractures filled with talc, carbonates, or tremolite develop preferentially from the boundary to the interior of the serpentinite body, whereas fractures are less common in the crustal rocks (metapelite, metabasaltic rocks) surrounding the

ultramafic body (Tarling et al. 2019a, b; Okamoto et al. 2021; Oyanagi et al. 2023; Figs. 4a, b, 5a–c; Table 1). Asymmetric fracturing between ultramafic bodies and metapelites is investigated by the DEM modeling of Okamoto et al. (2021; Fig. 12). In their model, the serpentinite body is surrounded by metapelite (unreacted matrix), and the metasomatic dehydration reaction is simplified to mineral A + S → Mineral B + H_2O, where S is a metasomatic agent such as Si (Fig. 12a). The reaction rate is defined as a function of S concentration, and the model deals with the advective fluid flow and diffusion of agent S. The results show that the solid volume-increasing reaction (Fig. 12b) preferentially causes radial fracturing around the serpentinite body, whereas in the solid volume-decreasing reaction (Fig. 12c) the branching fracture networks develop only within the serpentinite body. A comparison of the fracture patterns produced by numerical simulations (Okamoto et al. 2021) with natural vein networks in serpentinite (Okamoto et al. 2021; Oyanagi et al. 2023) suggests that metasomatic reactions in the serpentinite body were related to the solid volume decrease, given the greater amount of Mg released than Si gained. Dry mantle peridotite can be directly metasomatized (R3, R5), but natural occurrences suggest that hydration (serpentinization) often predates the Si-metasomatism (Table 1); therefore, the Si-metasomatism is characterized by dehydration (R1; R12; Oyanagi et al. 2015, 2020; Tarling et al. 2019b; Okamoto et al. 2021). Even if the solid volume decreases, the total volume (including fluids) increases with the progress of the metasomatic reaction (Okamoto et al. 2021). The evolution of the pore fluid pressure during dehydration is complicated, as it not only involves the rate of fluid production but also involves the rate of fluid release as well as the formation and destruction of porosity (Connolly 1997; Miller et al. 2003). However, given the low permeability of metasediments and metagabbro surrounding serpentinite, it is possible that high pore-fluid pressures are established in the serpentinite body due to dehydration induced by metasomatism, which is consistent with the presence of microstructures in veins that indicate precipitation in open pores (Tarling et al. 2019b; Okamoto et al. 2021).

The DEM models are very powerful for investigating the interaction of reactions and mass transport, but are still very simplified; e.g., they do not consider differential stress or plastic deformation, and the reaction rate is only a function of the concentration of a single metasomatic agent or fluid pressure (e.g., Okamoto et al. 2021). In addition, it is unclear how grain-scale processes can be linked to the outcrop scale and subduction zone scale. Further development of DEM models, linking them to realistic geochemical models, and regional scale numerical models will increase our understanding of the dynamic behaviors of the complex processes involving reactions, chemical transport, plastic deformation, fracturing, and fluid flow at the slab–mantle interface.

5.4 Implications of Mg- and Si-metasomatism for the mechanical properties of the subduction interface

Thermodynamic calculations (Figs. 7, 8, 9, 10; Okamoto et al. 2021; Collido et al. 2022b) show that the Mg-metasomatism of metasedimentary rocks occurs in warm subduction zones (e.g., Nankai and Cascadia), whereas it may be limited in cold subduction zones (e.g., NE Japan; Fig. 10). The source of the Mg-metasomatism is derived from mantle wedge serpentinite, suggesting that the chloritization of crustal lithologies could occur pervasively at contact with mantle rocks in warm subduction zones. Chlorite contains ~ 13 wt% H_2O and is stable up to 5.0–6.2 GPa (van Keken et al. 2011; Hermann and Lakey 2021), and Chl-rich reaction zones of 10–100 m thick are predicted to occur at the slab–mantle interface (Spandler et al. 2008; Marschall and Schumacher 2012). Thus, the formation of chlorite in crustal lithologies influences the global water budget, especially in warm subduction zones, where significant Mg mobility is expected. In contrast, as the element mobilities in the cold subduction zones are lower than those in the warm subduction zones, the bulk rock compositions of the mantle or crustal rocks influence directly the mineralogy of the products of fluid-rock interactions.

The seismic velocity structure and thermodynamic calculations suggest that the corner of the forearc mantle wedge is highly serpentinized (e.g., Bostock et al. 2002; Kato et al. 2011). In contrast, it is difficult to determine the thickness of the metasomatic reaction zones at the slab-mantle interface based on geophysical observations. Kim et al. (2013) investigated the seismic velocity structure of the subduction zone in central Mexico, and proposed that a talc layer of ~ 4 km thickness has been generated in the mantle wedge at 45 km depth. Talc has a low frictional coefficient and is velocity-strengthening to -neutral (e.g., Hirauchi et al. 2020; Moore and Lockner 2011). Deformation experiments suggest that even a few tens of percent of talc significantly reduces the bulk mechanical strength of a rock (Escartin et al. 2008; Moor and Lockner 2011; Hirauchi et al. 2012). Based on the thermodynamic constraints on talc stability, Peacock and Wang (2021) proposed that the strength of the slab–mantle interface may be related to the stability of talc. In contrast to talc, the deformation experiments of chlorite are limited. A recent shear experiment on chlorite (Okamoto et al. 2019) revealed that chlorite is frictionally weak (a coefficient of friction of 0.2–0.3 at $T \leq 400$ °C and 0.3–0.4

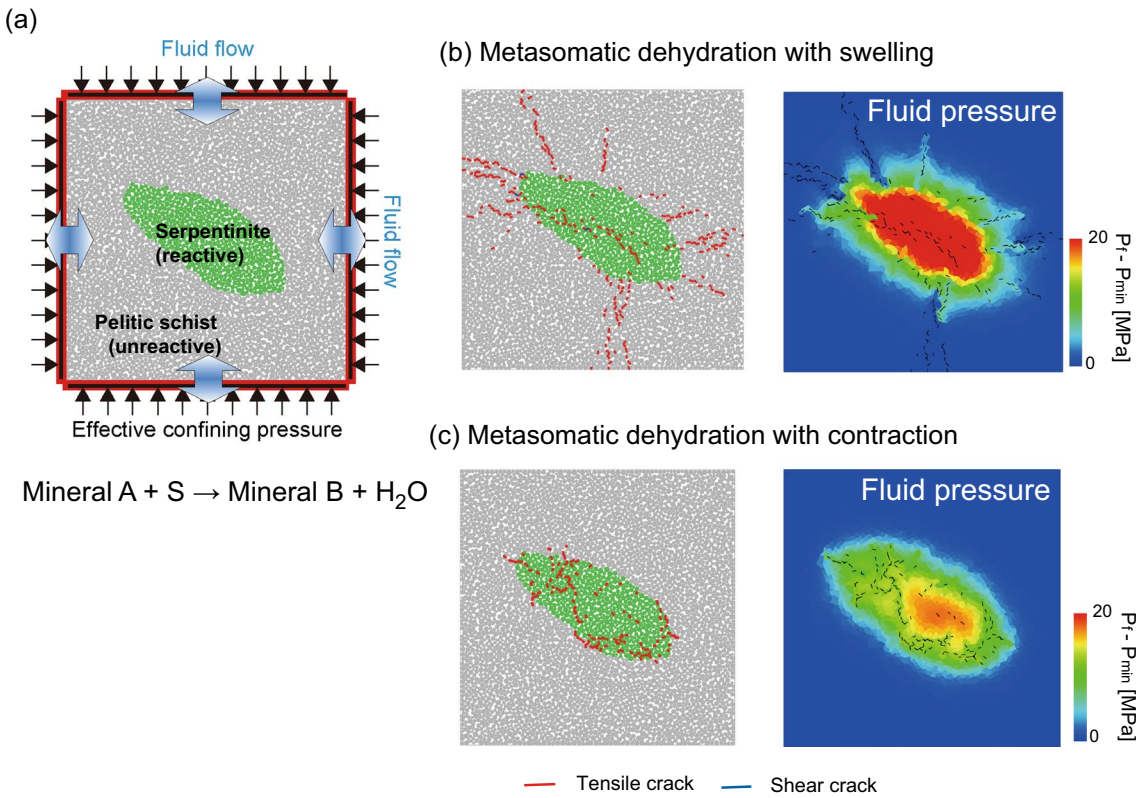

Fig. 12 Results of distinct element method (DEM) models of reaction-induced fracturing of serpentinite during metasomatism (modified after Okamoto et al. 2021). **a** Rock model composed of the reactive serpentinite surrounded by unreactive pelitic schist. **b**–**c** Fluid pressure and reaction ratio of (**b**) solid volume-increasing and (**c**) solid volume-decreasing metasomatic reactions. In the model, the reaction rate is a function of the concentration of the metasomatic agent S (e.g., silica), which is transported by diffusion. Branching fractures into the serpentinite body are produced during the solid volume-decreasing reactions. P_f = fluid pressure, P_{min} = minimum fluid pressure in the model

at 500–600 °C) and a behavior of velocity strengthening to neutral, meaning that chlorite fault rock is aseismic, as similar to talc.

In warm subduction zones such as Nankai and Cascadia, episodic tremor and slip (ETS) is observed around the slab-mantle interface near the mantle wedge corner, which is extensively serpentinized (e.g., Beroza and Ide 2011; Kato et al. 2010; Gao and Wang 2010). Although several mechanisms have been proposed, involving various processes, including silica precipitation (Audet et al. 2009), the mineralogy and fluid pressure within serpentinite (Mizukami et al. 2014; Hirauchi et al. 2022), dehydration-induced heterogeneity within eclogitic oceanic crust (e.g., Behr et al. 2018), and metasomatic reactions (Tarling et al. 2019a, b; Okamoto et al. 2021; Hoover et al. 2022; Ujiie et al. 2022), the relationship between the fluid-mediated reactions and ETS are still controversial. As described above, the metasomatic minerals between mantle-crust interfaces, such as talc, chlorite and tremolite, are related to stable slip related to strain hardening (e.g., Hirauchi et al. 2012). However, the dynamic mechanical behaviors during metasomatic reactions could be more complicated. Hoover et al. (2022) investigated the amphibole microstructures in the talc-bearing and talc-absent metasomatic rocks, and proposed that the talc-bearing sample represents the high-strain rates related to episodic slow slip, whereas talc-absent rocks show intervening aseismic creep. As discussed in the previous section, the metasomatized parts of the hydrated mantle are commonly fractured, forming vein networks of talc, tremolite, and carbonates (Tarling et al. 2019b; Okamoto et al. 2021; Hirauchi et al. 2022; Oyanagi et al. 2023; Figs. 4b, c, 5a–c, f). Metasomatic dehydration reactions with a solid volume change could involve the tensile to shear fractures and build-up of high fluid pressures. The repeated brittle failures related to the metasomatic reactions and the viscos flow of the metasomatic products could represent an analogue of ETS (Tarling et al. 2019b; Okamoto et al. 2021). The relative mobility of Mg and Si and the thickness of the metasomatic reaction zones that developed within crustal and mantle sides are significantly controlled by the thermal structures of the subduction zones and the compositions of fluids (Figs. 7, 8, 9; Okamoto et al. 2021; Codillo et al. 2022a, b).

Although previous studies mainly focussed on the influences of the pore fluid pressure on the subduction zone seismicity, the compositions of the multi-component aqueous fluids on the subduction zone rheology and seismic activities should be more explored to links the global material circulation and dynamic behaviors of the Earth's interiors.

6 Conclusions

The slab–mantle boundary in subduction zones is characterized by steep geochemical gradients, where fluid-related alteration occurs. The supply of Si has been thought to drive chemical changes at the crust–mantle interface. The experiments analogue to the crust-mantle contact at the low-pressure resulted in the development of a reaction zone dominated solely by the diffusive transport of Si. In contrast, bi-directional diffusion of Si and Mg between crust and mantle, or the preferential formation of reaction zones in crustal rocks by Mg-metasomatism are ubiquitously observed in natural high-pressure metamorphic belts. The recent studies on geochemical calculations using updated thermodynamic databases and the new geochemical modeling in this study reveal that near the surface and in cold subduction zones, dissolved Si is dominant in crust-derived fluids, whereas under mantle wedge conditions in warm subduction zones, the dissolved Mg content in mantle-derived fluids is as high as or even higher than that of Si in crust-derived fluids. This result is consistent with the natural occurrences of the metasomatic reaction zones in the metamorphic terranes, in which chlorite rocks commonly develop on the crustal side of the interface rather than in the talc zone on the serpentinite side. The Si- vs. Mg- metasomatism shows contrasting properties in mineralogy (talc and chlorite), water budget (hydration and dehydration), as well as solid volume change at the slab-mantle interface; therefore it potentially provide significant influences on hydrology, element circulation and mechanical properties, seismic activities along the plate interfaces within the subduction zones.

Supplementary Information

The online version contains supplementary material available at https://doi.org/10.1186/s40645-023-00568-w.

Additional file 1. Supporting infomation.

Acknowledgements
The authors thank Ken-ichi Hirauchi, Masaoki Uno, Shunya Okino, Jun Muto, Mitsuhiro Toriumi, Kazuki Yoshida, Takayoshi Nagaya, Ikuko Wada and Dandar Otgonbayaar for fruitful discussions. The authors also thank the Nishida prize committee at JpGU for their encouragement to prepare this review article.

Author contributions
AO planned this review and wrote the manuscript. RO conducted the geochemical calculations and edited the manuscript.

Funding
This work was supported by JSPS KAKENHI grants 18KK0376, 21H01189, 22H05295, 22H04932, and 23K13194.

Availability of data and materials
Data sharing is not applicable to this article as no datasets were generated or analyzed during the study.

Declarations

Competing interests
The authors declare no competing interests.

Author details
[1]Graduate School of Environmental Studies, Tohoku University, 6-6-20, Aramaki-aza-Aoba, Aoba-ku, Sendai 980-8579, Japan. [2]School of Engineering and Science, Kokushikan University, 4-28-1 Setagaya, Setagaya-ku, Tokyo 154-8515, Japan. [3]Research Institute for Marine Geodynamics, Japan Agency for Marine-Earth Science and Technology (JAMSTEC), 2-15, Natsushima, Yokosuka 237-0061, Japan.

Received: 5 February 2023 Accepted: 2 July 2023
Published online: 18 July 2023

References

Andreani M, Luquout L, Gouze P, Godard M, Hoise E, Gibert B (2009) Experimental study of carbon sequestration reactions controlled by the percolation of CO_2-rich brine through peridotites. Environ Sci Technol 43:1226–1231
Andreani M, Daniel I, Pollet-Villard M (2013) Aluminum speeds up the hydrothermal alteration of olivine. Am Mineral 98:1738–1744
Aoya M, Endo S, Mizukami T, Wallis SR (2013) Paleo-mantle wedge preserved in the Sambagawa high-pressure metamorphic belt and the thickness of forearc continental crust. Geology 41:451–454
Audet P, Bürgmann R (2014) Possible control of subduction zone slow-earthquake periodicity by silica enrichment. Nature 510:389–392
Bach W, Paulick H, Garrido CJ, Ildefonse B, Meurer WP, Humphris SE (2006) Unraveling the sequence of serpentinization reactions: petrography, mineral chemistry, and petrophysics of serpentinites from MAR 15 N (ODP Leg 209, Site 1274). Geophys Res Lett 33:L13306
Bach W, Klein F (2009) The petrology of seafloor rodingites: insights from geochemical reaction path modeling. Lithos 112:103–117
Beard JS, Frost BR, Fryer P, McGraig A, Serle R, Ildefonse B, Zinin P, Sharma SK (2009) Onset and progression of serpentinization and magnetite formation in olivine-rich troctolite from IODP Hole U1309D. J Petrol 50:387–403. https://doi.org/10.1093/petrology/egp004
Bebout GE, Penninston-Dorland SC (2016) Fluid and mass transfer at subduction interface—the field metamorphic record. Lithos 240–243:228–258
Beroza GC, Ide S (2011) Slow earthquakes and nonvolcanic tremor. Annu Rev Earth Planet Sci 39:271–296
Boschi C, Früh-Green GL, Delacour A, Karson JA, Kelley DS (2006) Mass transfer and fluid flow during detachment faulting and development of an oceanic core complex, Atlantis Massif (MAR 30oN). Geochem Geophys Geosyst 7:Q01004. https://doi.org/10.1029/2005GC001074
Bostock MG, Hyndman RD, Rondenay S, Peacock SM (2002) An inverted continental Moho and serpentinization of the forearc mantle. Nature 417:536–538. https://doi.org/10.1038/417536a
Codillo EA, Klein F, Dragovic B, Marchall HR, Baxter E, Scambelluri M, Schwarzenbach E (2022a) Fluid-mediated mass transfer between mafic and ultramafic rocks in subduction zones. Geochem Geophys Geosys 23:e2021GC10206
Codillo EA, Klein F, Marschall HR (2022b) Preferential formation of chlorite over talc during Si-metasomatism of ultramafic rocks in subduction zones. Geophys Res Lett 49:e2022GL100218
Connolly JAD (1997) Devolatilization-generated fluid pressure and deformation propagated fluid flow during prograde regional metamorphism. J Geophys Res 102:18149–18173

Connolly JAD (2005) Computation of phase equilibria by linear programming: a tool for geodynamic modeling and its application to subduction zone decarbonation. Earth Planet Sci Lett 236:524–541
Connolly JAD, Galvez ME (2018) Electrolytic fluid speciation by Gibbs energy minimization and implications for subduction zone mass transfer. Earth Planet Sci Lett 501:90–102
Dandar O, Okamoto A, Uno M, Oyanagi R, Nagaya T, Brenjargal U, Miyamoto T, Tsuchiya N (2019) Formation of secondary olivine after orthopyroxene during hydration of mantle wedge: evidence from the Khantaishir Ophiolite, western Mongolia. Contrib Mineral Petrol 176:86. https://doi.org/10.1007/s00410-019-1623-1
Escartín J, Andreani M, Hirth G, Evans B (2008) Relationships between the microstructural evolution and the rheology of talc at elevated pressures and temperatures. Earth Planet Sci Lett 268:463–475. https://doi.org/10.1016/j.epsl.2008.02.004
Frantz JD, MaO HK (1979) Bimetasomatism resulting from intergranular diffusion II: prediction of multimineralic zone sequence. Am J Sci 279:302–323
Frost BR, Beard JS (2007) On silica activity and serpentinization. J Petrol 48:1351–1368. https://doi.org/10.1093/petrology/egm021
Galvez ME, Manning CE, Connolly JAD, Rumble D (2015) The solubility of rocks in metamorphic fluids: a model for rock-dominated conditions to upper mantle pressure and temperature. Earth Planet Sci Lett 430:486–498
Galvez ME, Connolly JAD, Manning CE (2016) Implications for metal and volatile cycles from the pH of subduction zone fluids. Nature 359:420–424
Gao X, Wang K (2010) Rheological separation of the megathrust seismogenic zone and episodic tremor and slip. Nature 543:416–419
Hacker BR, Peacock SM, Abers GA, Holloway SD (2003) Subduction factory 2. Are intermediate-depth earthquakes in subducting slabs linked to metamorphic dehydration reactions? J Geophys Res 108:B12030. https://doi.org/10.1029/2001JB001129
Hattori K, Wallis S, Enami M, Mizukami T (2010) Subduction of mantle wedge peridotites: evidence from the Higashi-Akaishi ultramafic body in the Sanbagawa metamorphic belt. Island Arc 19:192–207
Hermann J, Lakey S (2021) Water transfer to the deep mantle through hydrous, Al-rich silicates in subduction zones. Geology 49:911–915
Hirauchi K, den Hartog SAM, Spiers CJ (2012) Weakening of the slab–mantle wedge interface induced by metasomatic growth of talc. Geology 41:75–78. https://doi.org/10.1130/G33552.1
Hirauchi K, Fukushima K, Kido M, Muto J, Okamoto A (2016) Reaction-induced rheological weakening enables oceanic plate subduction. Nat Commun. https://doi.org/10.1038/ncomms12550
Hirauchi K, Yamamoto Y, den Hartog SAM, Niemeijer AR (2020) The role of metasomatic alteration on frictional properties of subduction thrusts: an example from a serpentine body in the Franciscan Complex California. Earth Planet Sci Lett 531:115967. https://doi.org/10.1016/j.epsl.2019.115967
Hirauchi K, Nagata Y, Kataoka K, Oyanagi R, Okamoto A, Michibayashi K (2021) Cataclastic and crystal-plastic deformation in shallow mantle wedge serpentinite controlled by cyclic changes in pore fluid pressures. Earth Planet Sci Lett 576:117232. https://doi.org/10.1016/j.epsl.2021.117232
Hoover WF, Condit CB, Lindquist PC, Moser AC, Gurevara VE (2022) Episodic slow slip hosted by talc-bearing metasomatic rocks: high strain rates and stress amplification in a chemically reacting shear zone. Geophys Res Lett. https://doi.org/10.1029/2022GL101083
Huang F, Sverjensky DA (2019) Extended deep earth water for predicting major element mantle metasomatism. Geochim Cosmochim Acta 254:192–230
Hyndman RD, Peacock SM (2003) Serpentinization of the forearc mantle. Earth Planet Sci Lett 212:417–432. https://doi.org/10.1016/S0012-821X(03)00263-2
Jamtveit B, Austrheim H, Malthe-Sørenssen A (2000) Accelerated hydration of the Earth's deep crust induced by stress perturbations. Nature 408:75–78
Jamtveit B, Malthe-Sørenssen A, Kostenko O (2008) Reaction enhanced permeability during retrogressive metamorphism. Earth Planet Sci Lett 267:620–627
Johannes W (1969) An experimental investigation of the system MgO–SiO_2–H_2–CO_2. Am J Sci 267:1083–1104
Katayama I, Hirauchi K-I, Michibayashi K, Ando J-I (2009) Trench-parallel anisotropy produced by serpentine deformation in the hydrated mantle wedge. Nature 461:1114–1118
Kawahara H, Endo S, Wallis SR, Nagaya T, Mori H, Asahara Y (2016) Brucite as an important phase of the shallow mantle wedge: evidence from the Shiraga unit of the Sanbagawa subduction zone, SW Japan. Lithos 254–255:53–66. https://doi.org/10.1016/j.lithos.2016.02.022
Kelemen PB, Hirth G (2012) Reaction-driven cracking during retrograde metamorphism: olivine hydration and carbonation. Earth Planet Sci Lett 345–348:81–89
Kelemen P, Benson SM, Pilorge H, Psarras P, Wilcox J (2019) An overview of the status and challenge of CO_2 storage in minerals and geological formations. Front Clim 1:9. https://doi.org/10.3389/fclim.2019.00009
Kim YH, Clayton BW, Asimow PD, Jackson JM (2013) Generation of talc in the mantle wedge and its role in subduction dynamics in central Mexico. Earth Planet Sci Lett 384:81–87
King RL, Kohn MJ, Eiler JM (2003) Constraints on the petrologic structure of the subduction zone slab–mantle interface from Franciscan Complex exotic ultramafic blocks. Geol Soc Am Bull 115:1097–1109. https://doi.org/10.1130/B25255.1
Kita S, Okada T, Nakajima J, Matsuzawa T, Hasegawa A (2006) Existence of a seismic belt in the upper plane of the double seismic zone extending in the along-arc direction at depths of 70–100 km beneath NE Japan. Geophys Res Let 33:L24310. https://doi.org/10.1029/2006GL028239
Klein F, McCollom TM (2013) From serpentinization to carbonation: new insights from a CO_2 injection experiment. Earth Planet Sci Let 379:137–145. https://doi.org/10.1016/j.epsl.2013.08.017
Lacinska AM, Styles MT, Bateman K, Hall M, Brown PD (2017) An experimental study on the carbonation of serpentinite and partially serpentinized peridotites. Front Earth Sci 5:37. https://doi.org/10.3389/feart.2017.00037
Lichtner PC, Oelkers EH, Helgeson HC (1986) Interdiffusion with multiple precipitation/dissolution reactions: transient model and the steady-state limit. Geochim Cosmochim Acta 50:1951–1966. https://doi.org/10.1016/0016-7037(86)90251-6
Malthe-Sørenssen A, Jamtveit B, Meakin P (2006) Fracture patterns generated by diffusion controlled volume changing reactions. Phys Rev Lett 96:245501
Manning CE (1994) The solubility of quartz in H_2O in the lower crust and upper mantle. Geochim Cosmochim Act 58:483104839
Manning CE (1995) Phase-equilibrium controls on SiO_2 metasomatism by aqueous fluid in subduction zones: reaction at constant pressure and temperature. Int Geol Rev 37:1074–1093
Manning CE (2007) Solubility of corundum + kyanite in H_2O at 700 °C and 10 kbar: evidence for Al–Si complexing at high pressure and temperature. Geofluids 7:258–269
Manning CE (1997) Coupled reaction and flow in subduction zones: silica metasomatism in the mantle wedge. In: Jamtveit B, Yardley BWD (eds) Fluid flow and transport in rocks. Chapman and Hall, London, pp 139–148
Marschall HR, Schumacher JC (2012) Arc magmas sourced from mélange diapirs in subduction zones. Nat Geosci 5:862–867. https://doi.org/10.1038/ngeo1634
Menzel MD, Garrido CJ, Sánchez-Vizcaíno VL (2020) Fluid-mediated carbon release from serpentinite-hosted carbonates during dehydration of antigorite-serpentinite in subduction zones. Earth Planet Sci Lett 531:115964
Miller SA, van der Zee W, Olgaard DL, Connolly JADA (2003) fluid-pressure feedback model of dehydration reactions: experiments, modeling, and application to subduction zones. Tectonophysics 370:241–251
Miller DP, Marschall HR, Schumacher JC (2009) Metasomatic formation and petrology of blueschist-facies hybrid rocks from Syros (Greece): implications for reactions at the slab-mantle interface. Lithos 107:53–67. https://doi.org/10.1016/j.lithos.2008.07.015
Miyazaki K (2001) Heterogeneous growth of cordierite in low P/T Tsukuba metamorphic rocks from central Japan. J Met Geol 19:155–164

Moore DE, Lockner DA (2011) Frictional strengths of talc-serpentine and talc-quartz mixtures. J Geophys Res Solid Earth 116:1–17. https://doi.org/10.1029/2010JB007881

Moore DE, Rymer MJ (2007) Talc-bearing serpentinite and the creeping section of the San Andreas fault. Nature 448:795–797

Mori Y, Nishiyama T, Yanagi T (2007) Chemical mass balance in a reaction zone between serpentinite and metapelites in the Nishisonogi metamorphic rocks, Kyushu, Japan: implications for devolatilization. Island Arc 16:28–39

Mori Y, Shigeno M, Nishiyama T (2014) Fluid–metapelite interaction in an ultramafic mélange: implications for mass transfer along the slab–mantle interface in subduction zone. Earth Planet Space 66:47

Muñoz-Montecinos J, Angiboust S, Garcia-Casco A, Glodny J, Bebout G (2021) Episodic hydrofracturing and large-scale flushing along deep subduction interfaces: implications for fluid transfer and carbon recycling (Zagros Orogen, southeastern Iran). Chem Geol 571:120173

Nagaya T, Okamoto A, Oyanagi R, Seto Y, Miyake A, Uno M, Muto J, Wallis SR (2020) Crystallographic preferred orientation of talc determined by an improved EBSD procedure for sheet silicates: Implications for anisotropy at the slab–mantle interface due to Si-metasomatism. Am Mineral 105:873–893

Nagaya T, Okamoto A, Kido M, Muto J, Wallis SR (2022) Dehydration of brucite + antigorite under mantle wedge conditions: insights from the direct comparison of microstructures before and after experiments. Contrib Mineral Petrol 177:87. https://doi.org/10.1007/s00410-022-01956-z

Nurdiana A, Okamoto A, Yoshida K, Uno M, Nagaya T, Tsuchiya N (2021) Multi-stage infiltration of Na- and K-rich fluids from pegmatites at mid-crustal depths as revealed by feldspar replacement textures. Lithos 388–389:106096

Ogasawara Y, Okamoto A, Hirano N, Tsuchiya N (2013) Coupled reactions and silica diffusion during serpentinization. Geochim Cosmochim Act 119:212–230. https://doi.org/10.1016/j.gca.2013.06.001

Okamoto A, Shimizu H (2015) Contrasting fracture patterns induced by volume-increasing and -decreasing reactions: implications for the progress of metamorphic reactions. Earth Planet Sci Lett 415:9–18

Okamoto AS, Verberne BA, Niemeijer AR, Takahashi M, Shimizu I, Ueda T, Spiers CJ (2019) Frictional properties of simulated chlorite gouge at hydrothermal conditions: implications for subduction megathrusts. J Geophys Res Solid Earth 124:4545–4565. https://doi.org/10.1029/2018JB017205

Okamoto A, Oyanagi R, Yoshida K, Uno M, Shimizu H, Satish-Kumar M (2021) Rupture of wet mantle wedge by self-promoting carbonation. Com Earth Env 2:151. https://doi.org/10.1038/s43247-021-00224-5

Okamoto A, Shimizu H, Fukuda J, Muto J, Okudaira T (2017) Reaction-induced grain boundary cracking and anisotropic fluid flow during prograde devolatilization reactions within subduction zones. Contrib Mineral Petrol 172:75. https://doi.org/10.1007/s00410-017-1393-6

Okamoto A, Nagaya T, Endo S, Mizukami T (2023) Ultramafic rocks from the Sanbagawa belt: records of mantle wedge processes. Elements, accepted.

Oyanagi R, Okamoto A, Hirano N, Tsuchiya N (2015) Competitive hydration and dehydration at olivine–quartz boundary revealed by hydrothermal experiments: implications for silica metasomatism at crust-mantle boundary. Earth Planet Sci Lett 425:44–54. https://doi.org/10.1016/j.epsl.2015.05.046

Oyanagi R, Okamoto A, Tsuchiya N (2020) Silica controls on hydration kinetics during serpentinization of olivine: insights from hydrothermal experiments and a reactive transport model. Geochim Cosmochim Acta 270:21–42. https://doi.org/10.1016/j.gca.2019.11.017

Oyanagi R, Uno M, Okamoto A (2023) Metasomatism at a metapelite-ultramafic rock contact at the subduction interface: insights into mass transfer and fluid flow at the mantle wedge corner. Contrib Mineral Petrol 178:27. https://doi.org/10.1007/s00410-023-02011-1

Oyanagi R, Okamoto A, Tsuchiya N (2018) Al-zoning of serpentinine aggregate in mesh texture induced by metasomatic replacement reactions. J Petrol. https://doi.org/10.1093/petrology/egy039

Peacock MS (1999) Hydrous minerals in the mantle wedge and the maximum depth of subduction thrust earthquakes. Geophys Res Lett 26:2517–2520

Peacock SM, Wang K (2021) On the stability of talc in subduction zones: a possible control on the maximum depth of decoupling between the subducting plate and mantle wedge. Geophys Res Lett 48:1–8. https://doi.org/10.1029/2021GL094889

Plümper O, Botan A, Los C, Yang L, Malthe-Sørenssen A, Jamtveit B (2017) Fluid-driven metamorphism of the continental crust govern by nanoscale fluid flow. Nature Gesci 10:685–691

Putnis A (2009) Mineral replacement reactions. Rev Mineral Geochem 70:87–124

Reed M (1982) Calculation of multicomponent chemical equilibria and reaction processes in systems involving minerals, gases and an aqueous phase. Geochim Cosmochim Act 46:511–528

Saishu H, Okamoto A, Otsubo M (2017) Silica precipitation potentially controls earthquake recurrence in seismogenic zones. Sci Rep 7:13337. https://doi.org/10.1038/s41598-017-13597-5

Scambelluri M, Rampone E (1999) Mg-metasomatism of oceanic gabbros and its control on Ti-clinohumite formation during eclogitization. Contrib Min Petrol 135:1–17

Scambelluri M, Cannao E, Gilio M (2019) The water and fluid-mobile element cycles during serpentine subduction. A review. Eur J Mineral 31:405–428

Schwarzenbach EM, Caddick MJ, Beard JS, Bodnar RJ (2016) Serpentinization, element transfer, and the progressive development of zoning in veins: evidence from a partially serpentinized harzburgite. Contrib Mineral Petrol 171:5. https://doi.org/10.1007/s00410-015-1219-3

Schwarzenbach EM, Vogel M, Früh-Green GL, Boschi C (2021) Serpentinization, carbonation, and metasomatism of ultramafic sequences in the Northern Apennine Ophiolite (NW Italy). J Geophys Res Solid Earth 126:e2020JB020619

Shibuya T, Komita T, Nakamura K, Takai K, Maruyama S (2010) Highly alkaline, high temperature hydrothermal fluids in the early Archean ocean. Precambrian Res 182:230–238. https://doi.org/10.1016/j.precamres.2010.08.011

Shimizu H, Okamoto A (2016) The roles of fluid transport and surface reaction in reaction-induced fracturing, with implications for the development of mesh textures in serpentinites. Contrib Mineral Petrol 171:1–18

Sieber MJ, Yaxley GM, Hermann J (2022) COH-fluid induced metasomatism of peridotite in the forearc mantle. Contrib Mineral Petrol 177:144. https://doi.org/10.1007/s00410-022-01905-w

Sieber MJ, Yaxley GM, Hermann J (2020) Investigation of fluid-driven carbonation of a hydrated, forearc mantle wedge using serpentine cores in high-pressure experiments. J Petrol 61:egaa035

Spandler C, Hermann J, Faure K, Mavrogenes JA, Arculus J (2008) The importance of talc and chlorite "hybrid" rocks for volatile recycling through subduction zones; evidence from the high-pressure subduction mélange of New Caledonia. Contrib Mineral Petrol 155:181–198. https://doi.org/10.1007/s00410-007-0236-2

Sverjensky DA, Harrison B, Azzolini D (2014) Water in the deep earth: the dielectric constant and the solubilities of quartz and corundum to 60 kb and 1200 °C. Geochim Cosmochim Acta 129:125–145

Taetz S, John T, Bröcker M, Spandler C, Stracke A (2018) Fast intraslab fluid-flow events linked to pulses of high pore fluid pressure at the subducted plate interface. Earth Planet Sci Let 482:33–43. https://doi.org/10.1016/j.epsl.2017.10.044

Tarling MS, Smith SAF, Scott JM, Rooney JS, Viti C, Gordon KC (2019a) The internal structure and composition of a plate-boundary-scale serpentinite shear zone: the Livingstone Fault, New Zealand. Solid Earth 10:1025–1047. https://doi.org/10.5194/se-10-1025-2019

Tarling MS, Smith SAF, Scott JM (2019b) Fluid overpressure from chemical reactions in serpentinite within the source region of deep episodic tremor. Nat Geosci 12:1034–1042

Tutolo RM, Luhmann AJ, Tosca NJ, Seyfried WE Jr (2018) Serpentinization as a reactive transport process: the brucite silicification reaction. Earth Planet Sci Lett 484:385–395

Ujiie K, Shigematsu N, Fagereng Å, Nishiyama N, Tulley CJ, Masyyama H, Mori Y, Kagi H (2022) Megathrust shear modulated by albite metasomatism in subduction mélanges. Geochem Geophys Geosys 23:e2022GC010569. https://doi.org/10.1029/2022GC010569

Uno M, Koyanagawa K, Kasahara H, Okamoto A, Tsuchiya N (2022) Volatile-consuming reactions fracture rocks and self-accelerate fluid flow in the

lithosphere. Proc Nat Acad Sci USA 119:e2110776118. https://doi.org/10.1073/pnas.2110776118

Van Keken PE, Hacker BR, Syracuse EM, Abers GA (2011) Subduction factory: 4. Depth-dependent flux of H_2O from subducting slabs worldwide. J Geophys Res 116:B01401. https://doi.org/10.1029/2010JB007922

Van Keken PE, Wada I, Abers GA, Hacker BR, Wang K (2018) Mafic high-pressure rocks are preferentially exhumed from warm subduction settings. Geochem Geophys Geosys 19:2934–2961. https://doi.org/10.1029/2018GC007624

Vitale-Brovarone AV, Sverjensky DA, Piccoli F, Ressico F, Giovannelli RD, Daniel I (2020) Subduction hides high-pressure sources of energy that may feed the deep subsurface biosphere. Nat Commun 11:3880

Yoshida K, Okamoto A, Shimizu H, Oyanagi R, Tsuchiya N, Oman Drilling Project Phase 2 Science Party (2020) Fluid infiltration through oceanic lower crust in response to reaction-induced fracturing: Insights from serpentinized troctolite and numerical models. J Geophys Res 125:e2020JB020268. https://doi.org/10.1029/2020JB020268

Publisher's Note